New Theranostic Radionuclides for Metastatic Bone Disease

Biodistribution and Dosimetric Analysis

Dissertation

zur Erlangung des Doktorgrades (PhD)

der Medizinischen Fakultät

der Rheinischen Friedrich-Wilhelms-Universität

Bonn

Ambreen Khawar

aus Rawalpindi, Pakistan

2019

Angefertigt mit der Genehmigung

der Medizinischen Fakultät der Universität Bonn

1. Gutachter: Prof. Dr. Dr. Ralph A. Bundschuh
2. Gutachter: Prof. Dr. Frank Roesch

Tag der Mündlichen Prüfung: 08.10.2019

Aus der Klinik und Poliklinik für Nuklearmedizin

Direktor: Prof. Dr. med. Markus Essler

Dedicated to my husband and children

Index

1 Introduction

The term theragnostics (theranostics) was first used to describe use of information from imaging techniques for optimal treatment planning for an individual patient in oncology in 2005 (Bentzen, 2005). The term ‘theranostic’ in nuclear medicine is the combination of therapy and diagnostics while utilizing one drug formulation. The use of same drug formulation or molecular targeting vector labeled with diagnostic radionuclide (gamma or positron emitter) and therapeutic radionuclide (beta, alpha or auger electron emitter) allows molecular target specific delivery of radionuclide therapy in that patient. The tremendous increase in feasible production of diagnostic and therapeutic radionuclides for clinical use has made theranostic applications of nuclear medicine techniques better and presents possibility of cost effective personalized treatment (Bozkurt and Özcan., 2018). To achieve theranostic goal diagnostic radionuclide is believed to have the following properties (Dash et al., 2013; Taïeb et al., 2016)

- It may help in evidence based optimal patient selection for radionuclide therapy owing to possibility of better and reliable pre-therapeutic assessment of disease (molecular target) burden and tumor heterogeneity by generation of low noise/ high resolution images.
- It has an appropriate half-life that may not result in high radiation absorbed dose in patients for repeated diagnostic imaging and on the other hand is capable of following pharmacokinetics of complementary therapeutic radionuclide.
- It is able to quantify and predict pre therapy radiation doses for therapeutic radionuclide.
- It is able to monitor disease and objectively assesses therapeutic efficacy or therapy outcome.

1.1 Overview of available theranostic radionuclides

The role of theranostic application of radionuclides dates back to 1940’s when for the first time ^{131}I was used for diagnosis as well as therapy of various thyroid disorders including differentiated thyroid carcinoma. It is now also considered first use of targeted molecular therapy directed against Na-I symporters (Verburg et al., 2014; Yordanova et

al., 2017a). The radionuclides that are in use with theranostic intent can be broadly classified into three categories.

1.1.1 Single radionuclide with dual emissions

Radionuclides with emission of gamma or bremsstrahlung in addition to β^- particles have been utilized as single combination for diagnosis and therapy. Bremsstrahlung images with pure β^- emitters like strontium-89 (^{89}Sr) (Breen et al., 1992) or Yttrium-90 (^{90}Y) (Wright et al., 2015) have been employed in the past however, poor quality images was major drawback in its theranostic implication.

With γ and β^- emissions for diagnosis and treatment of benign and malignant thyroid disorders [^{131}I]NaI is the most specific example of combined diagnosis and therapy in single radionuclide. Pre-therapeutic diagnosis, dosimetry and post-therapeutic follow up with [^{131}I]NaI paved the way to personalized therapy in patients with thyroid carcinoma (Verburg et al., 2014). The dual emission iodine-131 labeled compounds in small (diagnostic) and large (therapeutic) doses e.g., [^{131}I]I-MIBG for neuroendocrine tumors, [^{131}I]I-tositumomab for relapsed or refractory low grade follicular or B cell non Hodgkin lymphoma patients and [^{131}I]I-PSMA-1095 in metastatic castration resistant prostate carcinoma patients (mCRPC) are some of the other examples of theranostic use (Yordanova et al., 2017a).

[^{188}Re]Re-HEDP, [^{153}Sm]Sm-EDTMP and [^{117m}Sn]Sn-DTPA with dual emissions are used for bone pain palliation in patients with metastatic bone disease (Serafini, 2001). Likewise lutetium-177 (^{177}Lu) with γ and β^- emissions conjugated with peptides and macromolecule has also found wide diagnostic and therapeutic utilization in neuroendocrine tumors, lymphoma, metastatic bone pain palliation and mCRPC patients (Dash et al., 2015; Ahmadzadehfar, 2016).

1.1.2 Sister imaging/therapeutic isotopes

This includes combination of γ and β^- emitting isotopes as well as positron (β^+) and β^- emitting isotopes of same radionuclide for theranostics. The use of gamma emitting isotope for planar or SPECT imaging as surrogate for therapeutic isotope can be seen with ^{123}I/ ^{131}I utilization in differentiated thyroid carcinoma (Buscombe, 2007; Urhan et

al., 2007) ^{123}I/ ^{131}I MIBG for neuroendocrine tumors (Intenzo et al., 2007) and ^{123}I/ ^{131}I labeled MIP-1095 targeted diagnosis and therapy in mCRPC patients (Yordanova et al., 2017a).

Among positron/beta isotope pairs ^{124}I/^{131}I for differentiated thyroid carcinoma (Erdi et al., 1999; Nagarajah et al., 2017), ^{124}I/^{131}I-MIP-1095 for mCRPC (Zechmann et al., 2014) have been utilized. Recently new theranostic pairs ^{86}Y/^{90}Y (Rösch et al., 2017), ^{44}Sc/^{47}Sc and ^{64}Cu/^{67}Cu (Rösch et al, 2017) have been proposed for labeling biomolecules or peptides against molecular targets for diagnosis and therapy respectively. Theoretically β^+/ β^- isotope pairs are considered better than γ /β^- isotope pairs owing to capability of better resolution and quantitation of PET for theranostic use but are still under investigation.

1.1.3 Pair of different imaging and therapeutic radionuclides

Since early 1990s, indium-111 (^{111}In) labeled compounds as SPECT tracer are in use as imaging agents with complimentary β^- emitting therapeutic compounds labeled with Yttrium-90 (^{90}Y) and ^{177}Lu e.g., ^{111}In- labeled monoclonal antibodies as surrogate to ^{90}Y-MAb or ^{177}Lu-MAb for pre-therapeutic patient selection as well as therapy planning (Bander et al., 2005).

Owing to better imaging with PET tracers, positron emitter gallium-68 (^{68}Ga) labeled vectors for diagnosis and ^{90}Y/^{177}Lu labeled vectors for therapy have gained wide acceptance as theranostic pairs. ^{68}Ga/^{177}Lu labeled somatostatin analogues, prostate specific membrane antigen, and bone seeking macromolecules as theranostic pairs in neuroendocrine, prostate carcinoma and metastatic bone disease patients respectively are in use (Yordanova et al., 2017a). Among longer lived cyclotron/ generator produced positron emitters ^{64}Cu, ^{44}Sc, ^{89}Zr have also been proposed for labeling vectors and prospective dosimetry (Rösch and Baum, 2011).

1.2 Role of dosimetry in theranostics

According to The new European Council Directive 2013/59 article 56 (Chiesa et al., 2017).

"For all medical exposure of patients for radiotherapeutic purposes, exposures of target volumes shall be individually planned and their delivery appropriately verified, taking into account that doses to non-target volumes and tissues shall be as low as reasonably achievable and consistent with the intended radiotherapeutic purpose of the exposure".

1.2.1 Dosimetry of diagnostic radionuclides

As theranostics requires repeated use of diagnostic radionuclides for selection of right patient for right radionuclide therapy at right time and monitoring of therapy outcome, dosimetric analysis of these radionuclides is essential. Moreover, possible role in predicting pre-therapeutic dosimetric analysis for therapeutic radionuclide can provide information for probable incidence of clinically measureable complications of normal organs.

With rapid advancements in radiopharmacy a lot of new diagnostic radio-pharmaceuticals against molecular targets are being developed. Their translation into clinical practice requires comparison of biodistribution and radiation safety i.e., critical organ and effective dose resulting from diagnostic dose. Though animal biodistribution and dosimetric analysis is performed as part of pre-clinical studies and extrapolated for human subjects but these studies under or overestimate the radiation absorbed doses for humans and hence necessitate the human studies. Recent use of ^{124}I for determining post therapeutic doses for ^{131}I has opened a new venue for use of longer lived radionuclide labeled compounds to determine post therapeutic organ and tumor lesion radiation absorbed doses (Zechmann et al., 2014). ^{44}Sc and ^{86}Y are other nuclides that are proposed suitable for pre-therapeutic PET based therapeutic dose determination.

1.2.2 Dosimetry and precision/ personalized radionuclide therapy

The success of radionuclide therapy relies on adequate delivery of activity that is able to impart lethal damage to tumor tissue with tolerable level of side-effects to normal tissues (Ljungberg and Sjögreen Gleisner., 2016). Fixed doses versus personalized radionuclide therapies are under discussion since long. The role of dosimetric analysis in individual patient based radionuclide therapy that is prediction of administered radionuclide activity tailored to an individual patient which could result in adequate tumor

control while minimizing potential side-effects to normal tissues is imperative (Flux et al., 2018; Strigari et al., 2014). Review of pre and intra therapeutic dosimetry for targeted radionuclide therapy with ^{131}I, ^{177}Lu and ^{90}Y labeled compounds has clearly advocated the great potential of individual patient based information (Eberlein et al., 2017). It is further advocated that in order to explore complete potential of radionuclide therapy, biological effectiveness i.e., DNA damage and repair mechanisms and effect of number and frequency of therapy cycles on normal and tumor tissues need to be inferred along with absorbed doses to normal organs and lesions obtained from dosimetric analysis (Eberlein et al., 2017). The progression of radiation dosimetric analysis for calculation of radiation absorbed doses from level of organs to tissue regions of millimeters to hundreds of micrometers is considered a great potential for advanced patient-specific dose estimates. Non-uniformities in absorbed doses with in tumor as well as surrounding critical structures can be displayed as dose volume histograms (DVH). In external beam radiotherapy (EBRT) less than 10% of non-uniformity in absorbed dose across target volume is considered successful. Moreover, use of tumor control probability (TCP) and normal tissue control probability (NTCP) in conjunction with DVH facilitates optimization of treatment planning. It is proposed that similar concept of treatment planning with use of TCP, NCTP and DVH can also be utilized for optimal treatment planning with internal radionuclide therapy. Thus, patient-specific dosimetry and treatment planning of radiolabeled substances are necessary for establishing safety of treatment and estimation of absorbed dose-response relationships.

1.3 Medical Internal Radiation Dose (MIRD) system

MIRD committee of the Society of Nuclear Medicine provides the internal dosimetry schema and basic methodology for calculation of absorbed doses from internally administered radiopharmaceutical both for diagnosis and therapeutic purposes (Bolch et al., 2009). MIRD schema was originally published in 1968, revised in 1976 and republished as MIRD primer in 1988 and 1991. MIRD schema is based on the idea that every radionuclide containing organ is the source of radiation exposure of other organs and of itself. The fraction of the radiation energy absorbed in the target organ depends on the physical quality of radiation (α, β, γ) and on the geometric relationships between source and target (distance, shape, position). MIRD schema provides framework for

absorbed dose assessment for whole organs, tissue sub regions, voxelized tissue structures as well as individual cellular compartments (Bolch et al., 2009).

For calculation of absorbed dose to whole organs homogenous activity distribution is assumed in the source as well as target organs. The calculation of absorbed dose is governed by following equation (Bolch et al., 2009):

$$\boldsymbol{D_{r_T}} = \sum_{r_S} \boldsymbol{\tilde{A}(r_S)} \,.\, \boldsymbol{S(r_T \leftarrow r_S)} = \boldsymbol{A_0} . \sum_{r_S} \boldsymbol{\tilde{a}(r_S)} \,.\, \boldsymbol{S(r_T \leftarrow r_S)} \text{---------- Equation 1}$$

Where "D_{r_T}" is the mean energy imparted to target region (r_T) per unit tissue mass delivered by cumulative activity in source region(r_S), "$\tilde{A}(r_S)$" is the time-integrated cumulative activity or total number of nuclear transformations of radiopharmaceutical in source region (r_S), and "$S(r_T \leftarrow r_S)$" is radionuclide specific mean absorbed dose rate delivered to target region (r_T) after administration per unit cumulative activity present in source region (r_S). "$\tilde{a}(r_S)$" is the fraction of administered activity in source region. "A_0" is the administered activity.

S is radionuclide as well as age/ sex specific computational anatomical model based parameter. It is determined by equation 2 as follows (Bolch et al., 2009):

$$\boldsymbol{S(r_T \leftarrow r_S)} = \frac{\sum_i \boldsymbol{E_i Y_i \emptyset\,(r_T \leftarrow r_S)}}{\boldsymbol{m_{r_T}}} \text{----------Equation 2}$$

Where "E_i" is the mean or individual energy of ith nuclear transition, "Y_i" is the number of ith nuclear transition per nuclear transformation, "$\emptyset\,(r_T \leftarrow r_S)$" is the absorbed fraction i.e., the fraction of radiation energy E_i emitted within the source region r_S that is absorbed in the target region r_T and "m_{r_T}" is mass of target region.

Calculation of S value considers either pre constructed whole body computational phantoms representing the reference individuals of given age, sex, total body weight and height or a model based on segmented images of subject anatomy from CT or MRI images. The S values for all types of nuclei of many nuclides for combinations of source and target organs for a 70 kg standard human as well as models of infants, women, men, pregnant women and adolescents with relationships between organ and organ systems, including the masses have been tabulated. These extensive tables of S values

of various geometric models are now available from the Society of Nuclear Medicine in (OLINDA/EXM) commercially available software (Stabin, 2008).

Voxel based dosimetry is possible with application of MIRD schema to voxels defined in PET or SPECT images. With use of voxel based S values, three dimensional distribution of absorbed dose is generated using calculated mean absorbed dose per voxel for all voxels in segmented region of the organ of interest that can be tumor or a region with in tumor. As a result of non-uniformities in absorbed dose profile, mean absorbed dose is not adequate to interpret clinical results. Thus voxel dosimetry is used to generate dose-volume histograms and isodose contours. Similar to radiation treatment planning comparison of dose-volume histograms in tumor and surrounding normal tissue can help in estimation of probability of success for internal radionuclide therapy and can help in tailoring the therapeutic dose to achieve desired effect at the target (Bolch et al., 1999, 2009).

Dosimetric analysis thus requires (Eberlein et al., 2017; Flux et al., 2018; Lassmann and Eberlein, 2018):

Quantitative measurement of pharmacokinetics: The use of MIRD schema requires accurate determination of activity changes within source organs with respect to time and in turn cumulative activity calculation. Quantitative serial imaging with gamma or positron emission tomography camera at optimal time points according to MIRD pamphlet no 16 (Siegel and Thomas, 1999), blood and urine sample collection is usually performed. Photon attenuation, scatter, camera limitations, voxel-based calculation of the distribution of energy depositions as well as image analysis, including image registration, image segmentation, volume of interest delineation and classification of normal tissue structures and tumors in the images are some of the issues that are taken into account. However, SPECT/CT or PET/CT has improved the quantitative accuracy owing to CT based volume delineation for organ and lesion dosimetry.

Integration of time activity curve and absorbed dose calculation: After generation of time activity curves in source organs and tumor lesion, integration of time activity curves is done by optimal curve fitting. Kletting et al. has provided a proposal of obtaining optimal fit procedures (Eberlein et al., 2017). Cumulative activity and absorbed dose in target

organ can easily be determined using OLINDA/ EXM software. The software requires selection of suitable phantom which results in nuclide specific parameters and tabulated S values already entered in the buffer and is stored for further calculations. Further with input of pre-determined kinetic parameters as number of decays or cumulative activity in the organ of interest or organ system or after a possible curve fitting for integration on time activity data with OLINDA/ EXM software, absorbed doses to target organs can be calculated (Stabin, 2008).

Patient Specific Dose Calculation: Prediction of patient specific activities tailored to absorbed dose limits for organs at risk e.g., kidneys in case of [^{177}Lu]-based PRRT or bone marrow in case of bone pain palliating radionuclide therapies. It is also desirable to predict whether tumor absorbed doses are capable of delivering significant therapeutic effect. Further taking into account the biological effectiveness of absorbed dose, dose fractionation and low dose with effective therapeutic effect is determined (Ljungberg and Sjögreen Gleisner, 2016)

1.3.1 Nuclear medicine in management of bone metastasis

Bone metastasis is a serious complication of many solid tumors. It affects more than 75% of patients with breast and prostate cancer, and 15-40% of patients with other types of tumors (Fischer and Kampen, 2012; Macedo et al., 2017). Pain, pathological fractures, hypercalcemia, myelosuppression, spinal cord compression and nerve root lesions are the skeletal related events (SRE's) that result in increased morbidity, mortality and reduced quality of life in these patients. Incidence of SREs is reported to be every 3-6 months that increase in frequency with disease progression (Wade et al., 2015). The diagnosis of bone metastasis at an early stage followed by therapy improves survival and quality of life.

The role of nuclear medicine is well established for diagnosis, staging and assessment of treatment response of skeletal metastases with use of conventional skeletal scintigraphy, SPECT, PET, and hybrid SPECT/CT, PET/CT imaging (Qu et al., 2012; Yang et al., 2011). Among these PET/CT imaging has been found the most sensitive and specific. Radionuclide therapy with β^- and α emitting bone seeking radiopharmaceuticals for bone pain palliation is an important aspect in management of

bone pain palliation in patients with metastatic skeletal disease (Pandit-Taskar et al., 2004). The use of imaging radionuclide and cytotoxic radionuclide therapy targeted at prostate specific membrane antigen (PSMA) in mCRPC patients, a new chapter in theranostics has emerged. It has made image guided salvage treatment of advanced mCRPC by targeting extracellular domain of PSMA with radiopeptides that are internalized upon binding and offers optimal antitumor activity, while limiting toxicity (Kesavan et al., 2018) . With success of PSMA based theranostics in mCRPC, efforts are being made to explore new theranostic radiopharmaceuticals for bone metastasis.

1.3.2 Radiopharmaceuticals for imaging of bone metastasis

The radiopharmaceuticals in use for diagnosis of bone metastasis can broadly be classified into osteotropic and oncotropics. The osteotropic radiopharmaceuticals includes bone seeking radiopharmaceuticals which owing to their high affinity to calcium hydroxyl apatite bind at sites of active bone formation or increased osteoblastic activity. Thus, their binding to both benign and malignant increased bone turn over sites results in high sensitivity and low specificity. The use of hybrid imaging like SPECT/CT or PET/CT is encouraged that increases the specificity. Below table 1 summarizes the osteotropic radiopharmaceuticals in use (Cuccurullo et al., 2013; O'Sullivan et al., 2015).

Tracer	Radio pharmaceuticals	Advantages	Disadvantages
SPECT	Tc-99m MDP	Low cost production, easy availability, favorable dosimetry	Non-specific as accumulates at both benign and malignant site.
	Tc-99m HEDP		
	Tc-99m HMDP		
PET	F-18 NaF	High first pass extraction, high sensitivity for metastatic lesion	Less specificity for pure lytic lesions as well as in absence of hybrid imaging, Costly cyclotron production and less availability
	[^{68}Ga]Ga-EDTMP, DOTMP, BPAMD, NO2AP-BP	Easy onsite, less expensive generator production, have theranostic advantage of pairing with [^{177}Lu]Lu-bisphosphonates or [^{225}Ac]Ac-bisphosphonates for therapy	

Table 1: Osteotropic radiopharmaceuticals (Cuccurullo et al., 2013; O'Sullivan et al., 2015).

In contrast oncotropic radiopharmaceuticals are the one that show uptake in malignant cells. The uptake is governed by specific or non-specific mechanism. The specific uptake is related to targeted receptor imaging found specifically in certain tumors. Table 2 below shows the various oncotropic radiopharmaceuticals.

Tracers	Radiopharmaceuticals	Metastasis of tumor detected (mechanism)
Specific	[^{131}I]/ [^{121}I]I-MIBG	Pheochromocytomas, paragangliomas and Apudomas (Nor adrenaline analogue)
	[^{68}Ga]Ga-DOTATOC/ DOTATATE, [^{111}In]In-octreotide	Neuroendocrine tumors(Somatostatin analogues)
	[^{131}I]NaI	Differentiated thyroid carcinoma (Na-I symporters)
	[^{68}Ga]Ga-PSMA	Prostate carcinoma (outer domain PSMA receptor)
Non specific	[^{99m}Tc]Tc-MIBI/ tetrofosmin	Localizes due to increased perfusion and later internalization with in mitochondria thus uptake related to increased metabolic activity of tumor cells
	[^{201}Tl]Tl-chloride	Uptake mediated through Na-K ATPase pump thus indicates metabolism and viability of tumor cells
	[^{18}F]F-choline/[^{11}C]C-choline	Prostate carcinoma (By up-regulated activity of choline kinase their uptake and later phosphorylation occurs)
	[^{18}F]FDG	Uptake by a transport mechanism mediated by GLUT 1 (glucose transporter protein) followed by phosphorylation and no degradation, hence uptake in bone metastasis is via non-specific increased glucose utilization

Table 2: Oncotropic radiopharmaceuticals(Cuccurullo et al., 2013; O'Sullivan et al., 2015)

1.3.3 Radionuclide therapy for bone metastasis

Bone metastasis is a multifocal disease that results in severe bone pain at multiple sites. Systemic targeted radionuclide therapy provides benefit of cost effective bone pain palliation with minimal side effects. The palliating effect of these agents is mediated by their accumulation at reactive bone sites around bone metastasis resulting in high target-to non- target tissue ratio and a very low concentration in the surrounding normal bone and bone marrow. Their mode of interaction is by acting as calcium analogue or attaching to phosphate at osteoblastic sites. The main side effects of radionuclide therapy are myelosuppression and pain flare (Macedo et al., 2017). It is believed that radionuclide therapy causes sterilization of cells which produce inflammatory mediators that activate nociceptors resulting in pain palliation and

improved quality of life. Moreover, it is seen that repeated radionuclide therapy may result in tumoricidal effect as well. The therapeutic effect is dependent on type and energy of emissions (β^- or α) from the radionuclide. The efficacy increases with concomitant use with hormonal therapy, chemotherapy or bisphosphonates (Fischer and Kampen, 2012; Pandit-Taskar et al., 2004). Table 3 gives overview of the various radionuclides used for therapy.

Radionuclides		Half-life (days)	Maximum/ mean energy and maximum tissue range	Gamma emission	% Success rate
β^- emitter	[^{32}P]NaP	14.3	1.71/0.695 MeV, 8 mm	No	77-84
	[^{186}Re]Re-HEDP	3.7	1.07/.349 MeV, 1.1 mm	Yes	50-100
	[^{188}Re]Re-HEDP	0.7	2.12/- MeV, 3 mm	No	60-75
	[^{89}Sr]Sr-Chloride	50.5	1.46/0.58 MeV, 2.4 mm	Yes	60-84
	[^{153}Sm]Sm-EDTMP	1.9	0.81/0.23 MeV, 0.6 mm	Yes	62-74
	[^{177}Lu]Lu-EDTMP	6.7	0.497	Yes	86
α-emitter	[^{223}Ra]$RaCl_2$	11.4	28 MeV, <100 µm	No	Improved Overall survival
Conversion electrons	[^{117m}Sn]Sn-DTPA	13.6	0.2-0.3	Yes	75

Table 3: Therapeutic radionuclides for bone pain (Fischer and Kampen, 2012; Pandit-Taskar et al., 2004)

1.4 Zoledronate based new theranostic bisphosphonates

Since many years, bisphosphonates are in use for pain palliation and prevention of complications from skeletal metastases. Its anti-resorptive effect is a proven *in vivo* and

in vitro fact (Luckman et al., 1998). High rate of adsorption by bisphosphonates encouraged its labeling with theranostic radionuclides (Fellner et al., 2012). Alpha-hydroxy bisphosphonates like pamidronate and, in particular, alpha-hydroxy bisphosphonates containing a potent nitrogen-containing moiety like zoledronate represent next generations of bisphosphonates (Ebetino et al., 2011; Montalvetti et al., 2001; Russell, 2007). In addition to binding with hydroxyapatite structure of the bone, their interaction with the HMG CoA reductase pathway results in inhibition of farnesyl diphosphate synthase (FPPS) culminating in apoptosis of osteoclasts, hence exhibiting a biochemical target (Fellner et al., 2012). Among them, zoledronic acid has shown highest FPPS inhibition and best affinity to hydroxyl apatite making it a bisphosphonate of choice for labeling with diagnostic and therapeutic radionuclide (Russell, 2007). The bifunctional chelate DOTA has facilitated labeling of these bisphosphonates with Me-(III); ^{68}Ga and ^{177}Lu for diagnosis and treatment of skeletal metastatic disease respectively, thus achieving a chemical goal of new theranostic development (Meckel et al., 2017).

Lutetium-177 with a half-life of 6.73 days, a low range of its β^- particles with maximum energy ($E_{\beta max}$ = 497 keV), gamma emissions at energies of 112 keV (6.4%) and 208 keV (11%), and the possibility of cost effective large scale production with high specific activity and radionuclide purity has gained high acceptance as a therapeutic radionuclide (Dash et al., 2015). Owing to deposition of its β^- energy in the lesions and their close environment, it is best suited for small to medium sized tumor lesions when labeled with a suitable carrier (Balter et al., 2015). Moreover, ^{177}Lu labeled bisphosphonates allow for a good theranostic combination with their gallium-68 labeled imaging counter parts using positron emission tomography (PET) (Alavi et al., 2015).

Pre-clinical *in vitro* and *in vivo* studies with [^{68}Ga]Ga-DOTA^{ZOL} has shown high hydroxyapatite binding, good target to background ratio with fast renal clearance and overall skeletal uptake comparable to other ^{68}Ga labeled DOTA α-H and α-OH bisphosphonates as well as [^{18}F]Na-F (Meckel et al., 2017; Pfannkuchen et al., 2017). Moreover, *in vivo* biodistribution in a single patient of prostatic carcinoma reported intense uptake in skeletal metastatic lesions with lower activity in background and other normal organs in comparison with complimentary [^{68}Ga]Ga-PSMA image (Pfannkuchen

et al., 2017). Data from animal studies comparing the biodistribution and dosimetric analysis extrapolated for humans between [^{177}Lu]Lu-EDTMP and [^{177}Lu]Lu-DOTA^{ZOL} indicate a higher skeletal absorbed dose for [^{177}Lu]Lu-DOTA^{ZOL} as well and present it to be a better agent for radionuclide therapy of bone metastases (Yousefnia et al., 2015).

Acyclic bisphosphonates like EDTMP labeled with ^{68}Ga and ^{177}Lu labeled EDTMP i.e., [^{68}Ga]Ga-EDTMP (Fellner et al., 2011) and [^{177}Lu]Lu-EDTMP (Agarwal et al., 2015) (Yuan et al., 2013) have been assessed as theranostic bisphosphonates. Phase I and II studies with [^{177}Lu]Lu-EDTMP for pain palliation in patients with bone metastases secondary to breast and prostate carcinoma have delivered encouraging results (Agarwal et al., 2015; Alavi et al., 2015; Mazzarri et al., 2015; Shinto et al., 2014; Thapa et al., 2015;Yuan et al., 2013). Radiation dosimetry analysis has also shown its safety with low dose delivery to the kidneys in patients with breast carcinoma and mCRPC in comparison to other bone pain palliating agents in use (Bal et al., 2015; Balter et al., 2015; Sharma et al., 2017). However, the lower kinetic stability of [^{177}Lu]Lu-EDTMP requires a high ligand concentration which is a drawback. Also, [^{68}Ga]Ga-EDTMP showed lower skeletal accumulation compared to its [^{177}Lu]Lu-EDTMP analogue and could not be paired as a theranostic agent (Meckel et al., 2017).

Bisphosphonates conjugated to macrocyclic chelators such as BPAMD have also been labeled with ^{68}Ga and ^{177}Lu resulting in [^{68}Ga]Ga-BPAMD (Fellner et al., 2010) (Passah et al., 2017) and [^{177}Lu]Lu-BPAMD (Baum and Kulkarni, 2012; Fellner et al., 2010; Pfannkuchen et al., 2017; Rösch and Baum, 2011). These DOTA-conjugated theranostic bisphosphonates have shown excellent results and represent good theranostic pairs (Pfannkuchen et al., 2017).

Despite the great potential of labeled BPAMD as a theranostic pair, further radiopharmaceutical research demonstrated, that the NOTA-version [^{68}Ga]Ga-NO2AP^{BP} (^{68}Ga-1,4,7-triazacyclonone-1,4-diacetic acid) of that bisphosphonate not only allowed for more effective labeling with ^{68}Ga, but also demonstrated superior targeting quality (Holub et al., 2015; Passah et al., 2017). It is superior with high thermodynamic stability and kinetic inertness as compared to DOTA labeled ^{68}Ga bisphosphonates, labeling of which is less efficient and more vulnerable to experimental conditions. It was characterized with high skeletal uptake and less kidney uptake (Holub et al., 2015).

However, in pre-clinical animal biodistribution studies its therapeutic counterpart [^{177}Lu]Lu-NO2AP^{BP} was found inferior to [^{177}Lu]Lu-BPAMD with less affinity to skeleton (Bergmann et al., 2016). Thus [^{68}Ga]Ga-NO2AP^{BP} and [^{177}Lu]Lu-BPAMD were proposed as theranostic combination of the simple bisphosphonate. The preclinical studies with [^{68}Ga]Ga-NODAGA^{ZOL} have shown comparable results to[^{68}Ga]Ga-NO2AP^{BP} and was found superior to [^{68}Ga]Ga-DOTA^{ZOL}. Recently [^{68}Ga]Ga-NODAGA^{ZOL} and [^{177}Lu]Lu-DOTA^{ZOL} have also been reported as the most effective new bisphosphonate based theranostic radiopharmaceuticals (Bergmann et al., 2016; Holub et al., 2015; Meckel et al., 2017; Nikzad et al., 2013). However, this theranostics combination requires analysis of [^{68}Ga]Ga-NODAGA^{ZOL} in humans.

Literature based comparison of [^{68}Ga]Ga-DOTA^{ZOL}(Meckel et al., 2017) with [^{68}Ga]Ga-NO2AP^{BP} (Holub et al., 2015) revealed slightly less hydroxyapatite binding (92.7 ±1.3 % versus 93.8 ± 4.4%) and low bone uptake at 60 min p.i. (Standard uptake value (SUV) of 5.27 ± 0.62 versus 6.19 ± 1.27). The in vivo biodistribution of [^{68}Ga]Ga-DOTA^{ZOL} in male Wistar rats showed faster kidney clearance with peak uptake in less than 5 min followed by clearance in comparison to [^{68}Ga]Ga-NO2AP^{BP} that showed continuous uptake till 50 min followed by clearance through urinary bladder. However, SUV for kidneys at 60 min p.i was found to be higher for [^{68}Ga]Ga-DOTA^{ZOL} (0.53 ± 0.04) as compared to [^{68}Ga]Ga-NO2AP^{BP} (0.26 ± 0.09). Evaluation of [^{68}Ga]Ga-NO2AP^{BP} in female breast carcinoma patients already proved its excellent ability to detect lesions along with favorable radiation dosimetry with very low kidney absorbed dose (Passah et al., 2017). However, [^{68}Ga]Ga-DOTA^{ZOL} has not been evaluated clinically so far. Moreover, preclinical animal studies with alpha emitter [^{225}Ac]Ac-DOTA^{ZOL} has shown biokinetics similar to [^{68}Ga]Ga-DOTA^{ZOL} and [^{177}Lu]Lu-DOTA^{ZOL} and proposed its translational use with strategies to reduce nephrotoxicity, thus increasing the importance of theranostic use of [^{68}Ga]Ga-DOTA^{ZOL} (Pfannkuchen et al., 2018).

Hence, [^{68}Ga]Ga-DOTA^{ZOL} with benefit of low cost, onsite generator production of gallium-68 having biodistribution and skeletal uptake comparable with [^{177}Lu]Lu-DOTA^{ZOL} (Meckel et al., 2017) and [^{225}Ac]Ac-DOTA^{ZOL}(Pfannkuchen et al., 2018) suggests it to be better than [^{18}F]Na-F as potential theranostic tracer allowing for patient-

individual dosimetry. In this study we evaluated biodistribution and dosimetric analysis of [^{68}Ga]Ga-DOTA^{ZOL} and [^{177}Lu]Lu-DOTA^{ZOL} to determine their feasible use for theranostics in skeletal metastatic disease.

1.5 [^{44}Sc]Sc-PSMA-617: New theranostic radiopharmaceutical for metastatic castration resistant prostate carcinoma patients

Prostate carcinoma is the second common cancer among males. The prognosis of prostate carcinoma is good at early stage but becomes refractory to treatment in advanced stages. Survival decreases to 31% with advanced metastatic disease in soft as well as skeletal tissue (Ahmadzadehfar et al., 2016; Rahbar et al., 2016a). High abundance of prostate specific membrane antigen (PSMA) is found in all prostate carcinoma cells that up regulates in metastatic castration resistant prostate carcinoma (mCRPC) (Ahmadzadehfar, 2016; Lütje et al., 2015). Since past two decades various studies have been conducted to evaluate several small ligands directed against external domain of PSMA. High affinity small ligand PSMA-617 with high tumor to background ratio (Benešová et al., 2015) labeled with gallium-68 (^{68}Ga) for PET imaging and lutetium-177 (^{177}Lu) for therapy of mCRPC are in use as theranostic pair for mCRPC. Though [^{68}Ga]Ga-PSMA-617 has played important role in diagnosis, staging and treatment follow up of mCRPC with [^{177}Lu]Lu-PSMA-617, its short half-life of 1.13 h is a major limitation to determine pre [^{177}Lu]Lu-PSMA-617 therapeutic dosimetric analysis which has a half-life of 6.7 days. Moreover, in a recent pre-clinical comparison of [^{68}Ga]Ga-PSMA-617 with [^{177}Lu]Lu-PSMA-617, it has surfaced that in vivo binding and distribution also differs between the two (Umbricht et al., 2017).

With emerging concept of theranostic radionuclides in personalized medicine, cyclotron/generator produced long-lived PET radionuclides are proposed as better diagnostic radionuclide for theranostic use specially for pre therapeutic dosimetry (Baum and Kulkarni, 2012). Evidence of prolonged imaging till 23.5 h and better sensitivity to detect lesions by [^{44}Sc]Sc-DOTATOC with half-life of 3.9 h encouraged labeling of PSMA-617 with scandium-44 (Pruszyński et al., 2012; Singh et al., 2017). Recent comparison of in vivo kinetics and in vitro characteristics of cyclotron produced [^{44}Sc]Sc-PSMA-617 with [^{68}Ga]Ga-PSMA-617, [^{177}Lu]Lu-PSMA-617 and [^{68}Ga]Ga-PSMA-11

revealed similar kinetics of [^{44}Sc]Sc-PSMA-617 to [^{177}Lu]Lu-PSMA-617 in contrast to gallium-68 labeled agents (Umbricht et al., 2017). Long half-life (3.9 h) of scandium-44 gives added advantages of its possible transport to distant places from site of production (Pruszyński et al., 2012), feasible delayed imaging with [^{44}Sc]Sc-PSMA-617and sentinel node imaging prior to surgery for primary prostate carcinoma. But the most pertinent is that it presents as better candidate for pre [^{177}Lu]Lu-PSMA-617 therapy dosimetric assessment in mCRPC patients (Umbricht et al., 2017). However presence of high energy gamma rays (>909 KeV) is considered a drawback (Eppard et al., 2017). Hence, a detailed dosimetric analysis is required for establishing its safe use for purpose of diagnosis and prospective dosimetric analysis.

Therapeutic success in terms of objective response with decline in PSA levels to [^{177}Lu]Lu-PSMA-617 therapy in 70% of mCRPC patients has been described (Ahmadzadehfar et al., 2015; Gaertner et al., 2017). In another review >50% reduction of serum PSA level in 30%-70% of mCRPC patients along with 10%-32% non-responders to [^{177}Lu]Lu-PSMA-617 therapy have been reported (Emmett et al., 2017). To date no substantial reasoning for lack of response in this fraction of mCRPC patients is provided. However, it is proposed that high dose delivery to tumor lesions while maintaining safety and avoiding toxicity could be a potential solution in enhancing response in resistant population, thus emphasizing role of personalized dosimetry in these patients (Emmett et al., 2017). At present, for treatment with [^{177}Lu]Lu-PSMA-617 initial administered doses are based on previous experience with PRRT, and escalated according to ongoing individual experience of respective clinicians at various centers.

Expression of PSMA in small intestine, proximal renal tubules and salivary glands in addition to prostate carcinoma cells was found responsible for toxicity and side effects (Ahmadzadehfar et al., 2016; Fendler et al., 2017; Yordanova et al., 2017b). Several [^{177}Lu]Lu-PSMA-617 PRRT studies have revealed its safety and effectiveness. Incidence of grade 3 or 4 renal, hematological and salivary gland toxicity has been found to be low. Occasional cases of reversible or transient xerostomia or grade 2 hematological toxicity have been reported (Baum et al., 2016; Yordanova et al., 2017b).

Dosimetric analysis with low pre therapeutic and high post therapeutic dose of [^{177}Lu]Lu-PSMA-617 using planar / planar + SPECT imaging also reported kidneys,

salivary and lacrimal glands to be the organs at risk respectively (Delker et al., 2016; Fendler et al., 2017; Kabasakal et al., 2015; Kratochwil et al., 2016; Kulkarni et al., 2016; Okamoto et al., 2017). Use of [^{68}Ga]Ga-PSMA-617 as a surrogate radiation dosimetric evaluation agent also revealed similar kinetics but lower doses as compared to [^{177}Lu]Lu-PSMA-617 (Afshar-Oromieh et al., 2015) .

Use of both planar and planar + SPECT low dose [^{177}Lu]Lu-PSMA-617 and [^{68}Ga]Ga-PSMA-617 PET imaging have drawbacks and inherent limitations for predicting pre-therapeutic or intra-therapeutic radiation dosimetry. Pre-therapeutic dosimetric analysis using low dose [^{177}Lu]Lu-PSMA-617 planar/ planar +SPECT imaging requires in many countries hospital stay due to radiation protection issues, multiple time point imaging, blood sampling and urine sample collection, which is cumbersome to patients as well as the hospital staff exposing them with high radiation doses. Secondly it gives high organ absorbed doses and has inability to determine lacrimal gland doses. Last but not the least low dose radiation may not interpret the biokinetics of high doses of [^{177}Lu]Lu-PSMA-617 administered for therapy in patients owing to the presence of more unlabeled compound in therapeutic dose (Delker et al., 2016; Kabasakal et al., 2015; Pfestroff et al., 2015;). As mentioned earlier, [^{68}Ga]Ga-PSMA-617 is incapable to follow kinetics of PSMA beyond 4 h and also computes lower absorbed doses. Hence, longer lived PET nuclide ^{44}Sc labeled PSMA is seen as an alternative for pretherapeutic dosimetry and better dose planning in mCRPC patients. This study evaluated biodistribution, dosimetric analysis of [^{44}Sc]Sc-PSMA-617 in mCRPC patients as surrogate marker for pre [^{177}Lu]Lu-PSMA-617 therapy dosimetric analysis.

2 Materials and Methods

This PhD research work presents evaluation of theranostic potential of zoledronate based bisphosphonate [^{68}Ga]Ga-DOTA^{ZOL} and [^{177}Lu]Lu-DOTA^{ZOL} in metastatic disease patients. In addition [^{44}Sc]Sc-PSMA-617 in metastatic castration resistant prostate carcinoma (mCRPC) patients was evaluated. For this biodistribution and dosimetric analysis of [^{68}Ga]Ga-DOTA^{ZOL}, [^{177}Lu]Lu-DOTA^{ZOL} and [^{44}Sc]Sc-PSMA-617 was assessed. Moreover, prospective post therapeutic normal organ absorbed doses for [^{177}Lu]Lu-DOTA^{ZOL} and [^{177}Lu]Lu-PSMA-617 were determined by using pharmacokinetic data of [^{68}Ga]Ga-DOTA^{ZOL} and [^{44}Sc]Sc-PSMA-617 respectively.

The research work was conducted at Department of Nuclear Medicine, University Medical Center, Bonn from April 2016 to March 2019. The studies detailed under were carried out in accordance to ethical standards of institutional review board and therefore been performed in accordance with the ethical standards laid down in the 1964 Declaration of Helsinki from the World Medical Association and all subsequent revisions (1983) and its appropriate legal requirements. All patients gave their informed consent to all involved imaging and therapeutic procedures.

2.1 Patient Selection

A total of 14 patients (Pts) were enrolled, 05 Pts for [^{68}Ga]Ga-DOTA^{ZOL}, 04 Pts for [^{177}Lu]Lu-DOTA^{ZOL} and 05 patients for [^{44}Sc]Sc-PSMA-617 biodistribution and dosimetric analysis.

For [^{68}Ga]Ga-DOTA^{ZOL}, five patients (M: F; 4: 1) with skeletal metastatic disease secondary to breast carcinoma in female patients and bronchial and metastatic castration resistant prostate carcinoma (mCRPC) in male patients were injected intravenously (i.v.) with mean ± SD dose of 172.6 ± 20.07 MBq (4.66 mCi) of [^{68}Ga]Ga-DOTA^{ZOL}. Table 4 summarizes the patient characteristics below

	PT1	PT2	PT3	PT4	PT5	mean	SD
Age	83	83	66	64	64	72	10.07
Weight	76	76	85	82	82	80	4.02
Sex	M	M	F	M	M		
Hematocrit	0.4	0.41	0.34	0.39	0.37	0.38	0.03
Dose	152	150	181	190	190	172.6	20.07
Tumor	mCRPC	mCRPC	Breast	Bronchial carcinoma	Bronchial carcinoma		
Previous therapies received	AH*/ CT#/ [177Lu]Lu-PSMA-617	AH*/ CT#/ [177Lu]Lu-PSMA-617	CT# + local Iradiation	CT#/ denusomab, nivolumab	CT#/ denusomab, nivolumab		

Table 4: Patient characteristics in which biodistribution and dosimetric analysis with [^{68}Ga]Ga-DOTA^{ZOL} was studied

The biodistribution and dosimetric analysis of [^{177}Lu]Lu-DOTA^{ZOL} was studied in four male patients with metastatic skeletal disease secondary to metastatic castration resistant prostate carcinoma (mCRPC) or bronchial carcinoma. After confirming sufficient uptake in the bone metastases with [^{68}Ga]Ga-DOTA^{ZOL} - PET/CT, these patients were hospitalized for treatment with [^{177}Lu]Lu-DOTA^{ZOL} in the context of an individual treatment attempt as no other treatment options were left for these patients. All patients had normal kidney function confirmed by renal function tests as well as renal scintigraphy. Table 5 shows patient details along with the injected activities of [^{177}Lu]Lu-DOTA^{ZOL} and previous therapies received.

	PT1	PT2	PT3	PT4	mean	SD
Age	83	66	64	64	69.25	9.21
Weight	76	76	82	82	79	3.46
Hematocrit	0.4	0.4	0.4	0.37	0.39	0.01
Injected activity	6000	6000	5873	6000	5968.25	63.5
Tumor	mCRPC	mCRPC	Bronchial carcinoma	Bronchial carcinoma		
Previous therapies received	AH*/ CT#/ [177Lu]Lu-PSMA-617	AH*/CT#+ local Iradiation	CT#/ denusomab, nivolumab	CT# / denusomab, nivolumab		

Table 5: Subject details of patients receiving radionuclide therapy with [^{177}Lu]Lu-DOTA^{ZOL}*Antihormonal, #Chemotherapy

Five men with progressive mCRPC enrolled for [^{177}Lu]Lu-PSMA-617 therapy and mean age of 69±2.2 years were enrolled for [^{44}Sc]Sc-PSMA-617 imaging. The details of injected activity as well as patient characteristics are given in table 6.

	PT1	PT2	PT3	PT4	PT5	mean	SD
Age	70	72	67	70	67	69	2.2
Weight	78	80	70	80	104	82.4	12.76
Hematocrit	0.33	0.30	0.39	0.30	0.29	0.32	0.04
Dose Injected Activity (MBq)	50.00	62.23	39.61	50.00	48.95	50.16	8.04
	0.64	0.78	0.57	0.63	0.47	0.62	0.11
PSA (ng/ml)	453.00	26.00	7.20	139.00	3000.00		
[^{177}Lu]Lu-PSMA cycles	3	1	2	----	1		
Other therapies received	RT$/ CT#/ AH*	AH*	RT$/ AH*and bisphosphonate therapy	RT$	RT$/CT#/ AH*		

Table 6: Subject details, injected radioactivity of [^{44}Sc]Sc-PSMA-617 and therapies received (~Hematocrit, *Antihormonal, #Chemotherapy, $Radiotherapy)

2.2 Preparation of radiopharmaceuticals

2.2.1 [^{68}Ga]Ga-DOTA^{ZOL}

Gallium-68 was obtained from a 1.85 GBq (50mCi) ^{68}Ge/^{68}Ga-generator (iThemba Labs; South-Africa). Radiolabeling of DOTA^{ZOL} obtained from ITG (Isotope Technologies Garching GmbH, Garching, Germany) was performed on a cassette module (Gaia, Elysia-Raytest GmbH, Germany). Development of silica TLC-plates was conducted in acetylacetone/acetone (1:1) for iTLC-plates. A radiochemical yield of ≥ 98% and radiochemical purity of ≥ 97% was obtained.

2.2.2 [^{177}Lu]Lu-DOTA^{ZOL}

DOTA^{ZOL} was radiolabeled in 0.8 ml ascorbic buffer (210 mg Na-L-ascorbat + 42 mg gentisic acid in 1 ml 0.05 N HCl) with non-carrier-added lutetium-177, both obtained from ITG Isotope Technologies Garching GmbH. The manual synthesis was carried out on a thermoshaker at a temperature of 95°C for 30 min. An aliquot of the product was taken and the quality control was carried out with silica-gel coated aluminium TLC-plates (silica 60 F 254.5x4.5 cm, Merck, Darmstadt, Germany). Analysis was performed with a single trace radioTLC-scanner (PET-miniGITA, Elysia-Raytest, Straubenhardt, Germany) and evaluation software (GinaStar TLC, Elysia-Raytest, Straubenhardt, Germany). Development of TLC-plate was conducted in 0.1 M citrate buffer (pH 4), where [^{177}Lu]Lu-DOTA^{ZOL} was found at R_f: 0-0.1, disaggregated DOTA at R_f: 0.5, and unlabeled lutetium-177 at R_f:1. The second TLC-plate was developed in a mixture of acetylacetone, acetone and HCl (1:1:0.1), where [^{177}Lu]Lu-DOTA^{ZOL} was found at R_f: 0-0.1 and unlabeled lutetium-177 at R_f:1. A radiochemical yield of ≥95% and a radiochemical purity ≥98% was obtained.

2.2.3 [^{44}Sc]Sc-PSMA-617

3 ml of scandium-44 obtained after post processing according to literature of eluted ^{44}Sc from prototype 185 MBq (5 mCi) ^{44}Ti/^{44}Sc generator (Mainz) was used to label GMP-grade PSMA-617 obtained from ABX (Radeberg, Germany). Quality control for radiochemical yield & purity was checked using TLC with 0.1M sodium citrate; ITLC with1:1 v/v 1 M ammonium acetate/methanol and HPLC with Nucleodur 100-3 C18 ec

125/4; Macherey-Nagel GmbH & Co. KG, Germany. A radiochemical yield of 98% and radiochemical purity of 99% was obtained (Eppard et al., 2017)

2.3 Data collection

To study biodistribution of radiopharmaceuticals, blood and urine samples were obtained along with image acquisitions after intravenous injection of radiopharmaceuticals. The protocol followed for image acquisition is summarized as follows

- PET/CT acquisition studies for PET radiopharmaceuticals
- Planar whole body gamma camera scintigraphy for gamma emitting radio-pharmaceutical

2.3.1 PET/CT Acquisition protocol for [^{68}Ga]Ga-DOTA^{ZOL} and [^{44}Sc]Sc-PSMA-617

Siemens Biograph 2 PET/CT scanner with a 58.5 cm axial field of view and a 16.2 cm longitudinal field of view was used for acquiring PET/CT images. The scanner has a spatial resolution of about 6 mm in axial and transversal direction (at a radius of 10 mm). All patients underwent a low dose CT scan (120kV, 40mAs) of abdomen for attenuation correction and patient positioning with kidneys in field of view. Initial dynamic imaging of abdomen for 30 minutes in list mode was performed starting simultaneously with i.v injection of [^{68}Ga]Ga-DOTA^{ZOL} or [^{44}Sc]Sc-PSMA-617. Later static skull to mid-thigh PET/CT images were acquired at 45 min and 2.5 h post injection (p.i.) for [^{68}Ga]Ga-DOTA^{ZOL} and at 45 min, 2 and 19.5 h p.i.. for [^{44}Sc]Sc-PSMA-617, each preceded by low dose CT examination for patient positioning and attenuation correction. Images were reconstructed using an iterative reconstruction algorithm (OSEM with 8 iterations, 16 subsets), application of Gaussian filter of 4mm and were corrected for scatter. The dynamic images were reconstructed into 6 images of 300s.

2.3.2 Planar whole body scintigraphy protocol with [^{177}Lu]Lu-DOTA^{ZOL}

Serial whole body planar scintigraphy (anterior and posterior views) was performed with dual head Symbia SPECT/CT system (Symbia T, Siemens Healthineers, Erlangen, Germany) at 20 min, 3, 24 and 167 h post injection (p.i). Acquisition was done

in supine position at a speed of 10 cm/min using LEHR collimators with 20% energy window centered at a photopeak of 208 keV. Images were processed using an iterative ordered subset maximization algorithm provided by the manufacturer into a matrix of 256*1024. The first data set obtained at 20 min (prior to voiding of the bladder) was considered as reference with 100% of administered activity. A standard source of known activity was placed between the legs in all images at the time of acquisition. For conversion of counts/min to activity, the gamma camera was pre-calibrated using a known activity of [^{177}Lu]Lu-DOTA^{ZOL} and imaging it at the same speed and distance of 10 cm/min.

2.3.3 Blood and Urine sampling

Blood and urine samples were drawn at varying time points (table 7). Urine samples were collected in pre weighed containers. A 1480 WIZARDTM 3n Gamma counter was used to measure activity of 1ml blood and urine of [^{68}Ga]Ga-DOTA^{ZOL} and [^{44}Sc]Sc-PSMA-617 and 0.2ml blood of [^{177}Lu]Lu-DOTA^{ZOL} samples along with known standards of respective radiopharmaceutical. The calibration factor determined from the standard activity measurement was used to determine the activity (MBq) of respective radiopharmaceutical in blood and urine samples.

Sample type	**[^{68}Ga]Ga-DOTA^{ZOL}**	**[^{44}Sc]Sc-PSMA-617**	**[^{177}Lu]Lu-DOTA^{ZOL}**
Blood	5, 10, 15, 20, 25, 30, 45 min and 2.5 h p.i.	5, 10, 15, 20, 25, 30, 45 min, 2 and 19.5 h p.i.	20 min, 3, 8, 24 and 167 h p.i
Urine	45 min and 2.5 h p.i.	45 min and 2 h p.i.	----------

Table 7 : Time points of blood and urine sample collection

2.4 Data analysis

The PET/CT dynamic and static acquisition data and whole body planar (anterior and posterior) scintigraphy images were analyzed qualitatively to assess the physiological and pathological uptake of [^{68}Ga]Ga-DOTA^{ZOL}, [^{44}Sc]Sc-PSMA-617 and [^{177}Lu]Lu-DOTA^{ZOL} respectively. The organs with increased tracer uptake were identified as source organs for further dosimetric analysis which were

- Kidneys, liver, spleen, urinary bladder, lumbar (L1-L3) vertebrae, salivary glands and whole body for [^{68}Ga]Ga-DOTA^{ZOL} as shown in illustration 1e.
- Kidneys, liver, spleen, urinary bladder, salivary glands and whole body for [^{44}Sc]Sc-PSMA-617 as shown in illustration 2.
- Kidneys, urinary bladder and skeleton for [^{177}Lu]Lu-DOTA^{ZOL} as shown in illustration 1a-d.

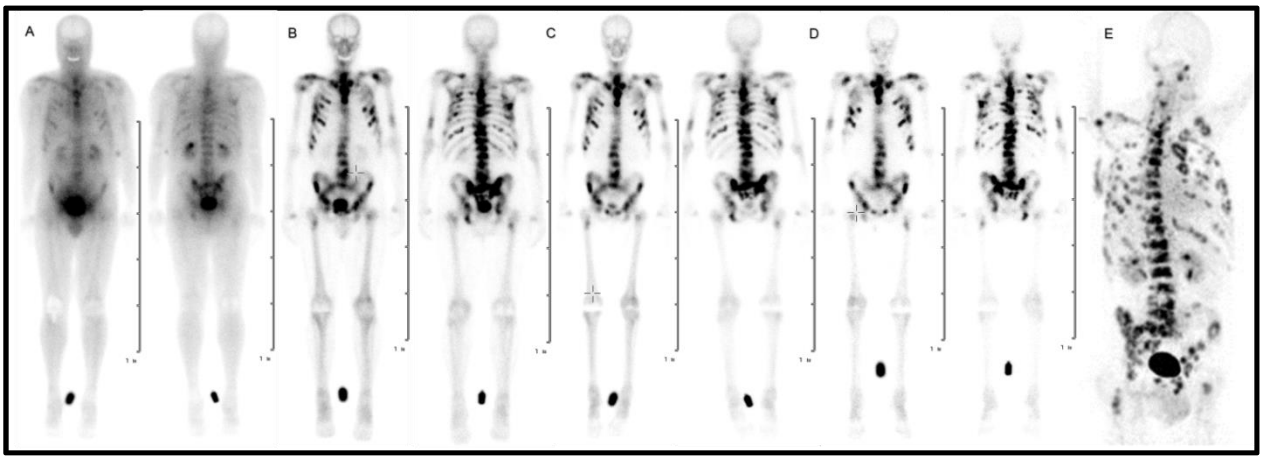

ill. 1: Planar scintigraphy (anterior and posterior views) after therapeutic application of [^{177}Lu]Lu-DOTA^{ZOL}at (a) 20 min, (b) 3 h, (c) 24 h, (d) 168 h and (e) PET/CT after application of [^{68}Ga]Ga-DOTA^{ZOL} in a patient with bone metastases secondary to bronchial carcinoma.

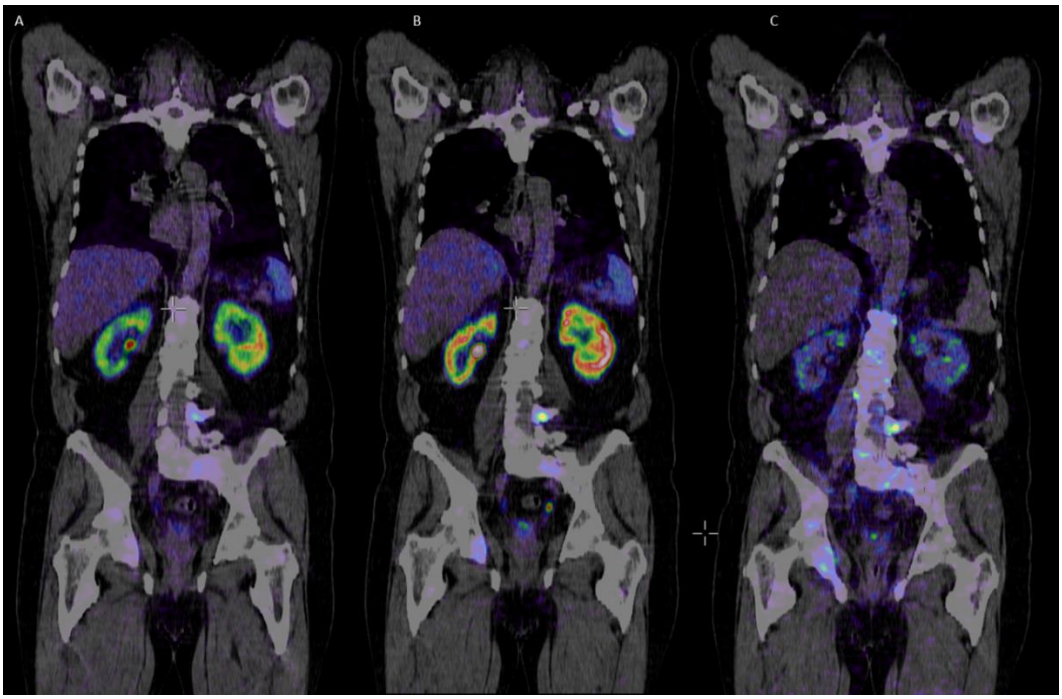

ill. 2: Distribution of [^{44}Sc]Sc-PSMA-617 at (A) 45min, (B) 2 h and (C) 19.5 h

Pharmacokinetics of respective radiopharmaceutical were assessed qualitatively and quantitatively by plotting % injected dose in source organs with respect to time. [^{68}Ga]Ga-DOTA^{ZOL} PET/CT images were compared visually to [^{68}Ga]Ga-PSMA-617, [^{18}F]-FDG PET/CT and [^{99m}Tc]Tc-MDP planar whole body images. Skeletal uptake kinetics were assessed by comparison of lesion to normal bone SUV ratio for representative metastatic lesions on [^{68}Ga]Ga-DOTA^{ZOL} with [^{68}Ga]Ga-PSMA-617 and [^{18}F]-FDG PET/CT.

2.4.1 Dosimetric analysis with [^{68}Ga]Ga-DOTA^{ZOL} and [^{44}Sc]Sc-PSMA-617

The dosimetric analysis was carried out in following steps

- Total source organ activity was calculated in MBq by multiplying the CT based source organ volume (ml) with mean counts/ml (KBq/ml) determined by drawing volume of interest (VOI) encompassing entire source organ on CT image using MEDISO interview fusion software (MEDISO Medical Imaging Systems, Buda-pest, Hungary) and dividing it with 1000. For [^{68}Ga]Ga-DOTA^{ZOL}, skeletal activity was calculated by multiplying the mean counts/ml in lumbar vertebrae with 5000 (total weight of skeleton in an adult) (ICRP, 1995).
- Percent of injected activity in all source organs was determined. For % of injected activity in whole body, as legs and some part of upper arms was not imaged, hence instead of using total injected dose in its calculation we used estimated injected dose in image only. We assumed initial homogenous tracer distribution and scaled the injected activity proportional to % weight of body in image by using equation 3. Percent body weight in image was calculated by using equation 4.

$$\%\ \mathbf{Whole\ body\ activity(t)} = \frac{\mathbf{Activity\ in\ static\ (skull-midthigh)image\ (t)\times 100}}{\mathbf{scaled\ injected\ activity\ in\ image}}$$ -------Equation 3

$$\%\ \mathbf{Body\ weight(image)} = \frac{\mathbf{CT\ volume\ of\ whole\ bodyimage\times mean\ CT\ density\times 100}}{\mathbf{patient\ weight}}$$ --Equation 4

- OLINDA/EXM version 2.0 (Hermes Medical Solutions, Stockholm, Sweden) was used for generation of time activity curves and determination of residence time (MBq-h/MBq). For this fitting of mono exponential curve on whole body and salivary glands kinetics and bi exponential curves for kinetics of rest of source organs was done. Residence time for remainder of the body for [^{68}Ga]Ga-

DOTA^{ZOL} was calculated by fitting A × [1- exp$^{-\lambda t}$] function to cumulative urinary excretion and using method explained by M. G. Stabin (Stabin, 2008). The same for [^{44}Sc]Sc-PSMA-617 was calculated by subtracting residence time of all source organs except urinary bladder from whole body residence time.

- Indirect blood based method with patient hematocrit based red marrow to blood ratio (RMBLR) for calculating bone marrow self-dose (Hindorf et al., 2005; Sgouros et al., 2000; Shen et al., 1999; Siegel, 2005)
- To calculate residence time for urinary bladder contents, trapezoidal method was used taking into account urinary bladder activity in images along with activity in urinary samples.
- Organ absorbed doses and effective doses/ MBq were calculated with OLINDA/EXM version 2.0 (Hermes Medical Solutions, Stockholm, Sweden) after adjusting weight of organs for patient by multiplying the reference adult male/ female whole body weight with factor obtained by dividing patient weight with reference adult (male/female) weight respectively. The mean of residence times, organ absorbed doses (mSv/MBq) and effective doses (mSv/MBq) were calculated. The total effective dose in mSv received with usual injected dose of 150 MBq of [^{68}Ga]Ga-DOTA^{ZOL} and 50 MBq of [^{44}Sc]Sc-PSMA-617 was calculated by multiplying their mean effective dose (mSv/MBq) with injected activities respectively.

2.4.2 Post therapeutic absorbed dose calculation for [^{177}Lu]Lu-DOTA^{ZOL} and [^{177}Lu]Lu-PSMA-617 by mathematical extrapolation of pharmaco-kinetic analysis of [^{68}Ga]Ga-DOTA^{ZOL} and [^{44}Sc]Sc-PSMA-617

Total activity of [^{68}Ga]Ga-DOTA^{ZOL} and [^{44}Sc]Sc-PSMA-617 in source organs was extrapolated to a theoretical [^{177}Lu]Lu-DOTA^{ZOL} and [^{177}Lu]Lu -PSMA-617 activity at all imaging time points by applying equation 3-3.

$$\boldsymbol{Activity_{Lu\,Corrected}} = \boldsymbol{A(t)} \times \boldsymbol{e}^{\frac{0.693 \times t(h)}{T}} \times \boldsymbol{e}^{\frac{-0.693 \times t(h)}{161.52\,h}} \text{----------Equation 5}$$

Where T = physical half-life of ^{68}Ga or ^{44}Sc. In this equation, the physical decay component of ^{68}Ga or ^{44}Sc was removed by reverse decay correction to the time of injection

leaving only the biological decay component of $DOTA^{ZOL}$ or PSMA-617 respectively. By applying forward decay correction with the physical half-life of ^{177}Lu (161.52 h) theoretical [^{177}Lu]Lu-$DOTA^{ZOL}$ and [^{177}Lu]Lu-PSMA-617 kinetics were extrapolated for all imaging time points. In case of whole body activity calculation for [^{177}Lu]Lu-PSMA-617 above method was applied until the 2 h time point. Then physical decay correction for ^{177}Lu was carried forward from 2 h time point. Reason for this was to remove an error of increment in activity at the last 19.5 h time point for the whole body activity calculation. Likewise, activity (MBq)/ml data of blood and urine samples were treated in the same way as described for source organs as well.

Organ absorbed doses for [^{177}Lu]Lu-$DOTA^{ZOL}$ and [^{177}Lu]Lu-PSMA-617 were calculated by using total source organ activity computed by extrapolation following the same steps as described for dosimetric analysis of [^{68}Ga]Ga-$DOTA^{ZOL}$ and [^{44}Sc]Sc-PSMA-617. Considering normal tissue complications probability (NTCP) toxicity limits derived from external beam radiotherapy (EBRT) for organs at risk, maximum permissible activity (Gy) and the maximum number of therapy cycles of [^{177}Lu]Lu-$DOTA^{ZOL}$ and [^{177}Lu]Lu-PSMA-617 (6 GBq per cycle) that can be administered in each patient were determined.

2.4.3 Dosimetric analysis with [^{177}Lu]Lu-$DOTA^{ZOL}$

To measure the percent activity in source organs, cumulated activity in source organs (kidneys, urinary bladder) was determined. Percent injected activity in skeleton was determined by subtraction of percent injected activity in blood, urinary bladder and kidneys from percent injected activity in whole body activity.

For cumulated activity in source organ, whole body ROI's were drawn. A rectangular ROI was drawn near the head region above the shoulder for background measurement and an elliptical ROI was used for measurement of the standard source placed between the legs. ROI on adductor muscle was drawn for soft tissue reference. Same sized ROI's were replicated on serial images (kidneys ROI's up to the 24 h data set and all remaining ROI's in all subsequent image data sets). Background corrected counts in right and left kidney, soft tissue, urinary bladder and whole body were determined on anterior and posterior images. The geometric mean counts/min in all

source organs at all data time points was determined. Using EANM dosimetry committee (Hindorf et al., 2005) whole body activity at subsequent time points (T) was determined by multiplying the injected activity with the normalized geometric mean whole body counts at the respective time points as given in equation 6,

$$A_{WB,T} = A_0 . \frac{\sqrt{Anterior\ counts_T . Posterior\ counts_T}}{\sqrt{Anterior\ counts_t . Posterior\ counts_t}}$$ ----------Equation 6

where t = 20 min, T= subsequent time points and A_0 = initial injected activity. Likewise, activity in the urinary bladder was also determined by multiplying the injected activity with the normalized geometric mean counts in urinary bladder.

For calculation of activity in the right and left kidneys at all data points, a conjugate view method with a simple geometrically based subtraction technique described in MIRD pamphlet no 16 (Siegel and Thomas, 1999) by equation 7 was used,

$$A_j = \sqrt{\frac{I_A I_P}{e^{-\mu_e t}}} \frac{f_j}{C}$$ ----------Equation 7

where I_A = anterior count rate , I_P = posterior count rate, f_j represents source organ self-attenuation correction which was calculated from the source region linear attenuation coefficient μ_j and source thickness t_j using equation 8. Factor $\mu_e t$ represents the transmission factor across the patient thickness t in the area of the ROI with a linear attenuation coefficient μ_e calculated using equation 9. From [^{68}Ga]Ga-DOTA^{ZOL}- PET/CT of respective patient, CT based measurements of source organ thickness as well as whole body thickness and thickness anterior and posterior to source organs at same level were used. C is the calibration factor determined for gamma camera with a known standard source and was same in all the studies (Siegel and Thomas, 1999). For measurements of μ_j and μ_i (linear attenuation coefficients for whole thickness), we applied a CT based Hounsfield units method described by Kabasakal et al for [^{177}Lu]Lu-PSMA-617 dosimetric analysis (Kabasakal et al., 2015)

$$f_j = \frac{\left(\frac{\mu_j t_j}{2}\right)}{\sinh\left(\frac{\mu_j t_j}{2}\right)}$$ ----------Equation 8

$$\mu_e = \left(\frac{1}{t}\right) \sum_{i=1}^{n} \mu_i t_i = \mu_j + \left(\frac{1}{t}\right) \sum_{i=1}^{n} (\mu_i - \mu_j) t_i$$ ----------Equation 9

A simple geometric based background subtraction technique using equation 10 was used,

$$F = \left\{\left[1 - \left(\frac{I_{ADJ}}{I_A}\right)\left(1 - \frac{t_j}{t}\right)\right]\left[1 - \left(\frac{I_{ADJ}}{I_P}\right)\left(1 - \frac{t_j}{t}\right)\right]\right\}^{\frac{1}{2}}$$ ----------Equation 10

where I_{ADJ} is the count rate through the patient from a soft tissue area of same size as that of the organ ROI. I_A, I_P, t_j and t are the same a s previously defined (Siegel and Thomas, 1999).

OLINDA/EXM version 2.0 (Hermes Medical Solutions, Stockholm, Sweden) software was used for performing bi exponential kinetic analysis on percent injected activity in the whole body, kidneys and skeletal system at all data time points and calculation of residence times (MBq-h/MBq). Residence time for the skeletal system was assumed to be distributed equally between trabecular and cortical bone. Residence time for urinary bladder contents was determined by applying Cloutier's dynamic urinary bladder model with 4h voiding interval, total urinary fraction and effective half-life. For this urinary fraction at all time points was calculated by applying function A* $(1-e^{-\lambda T})$. Effective half-life was determined by fitting a logarithmic function to urinary excretion curve. Bone marrow self-dose was determined by using indirect blood-based method mentioned earlier. By subtracting residence times for kidneys, bone marrow and skeletal system from whole body residence time, the remainder of body residence time was calculated.

Residence time for kidneys, cortical and trabecular bone, urinary bladder contents, red marrow self-dose and remainder of body were used as an input in OLINDA/EXM version 2.0 (Hermes Medical Solutions, Stockholm, Sweden) software for calculation of organ absorbed doses and effective doses after adjusting the weight of patient organs as described earlier.

3 Results

The results of visual analysis, biokinetics and dosimetric analysis of three radiopharmaceuticals have been found encouraging for their use for diagnosis and therapy. The results are summarized below.

3.1 [^{68}Ga]Ga-DOTA^{ZOL}

3.1.1 Biodistribution and kinetic analysis

Visual analysis of PET/CT images revealed intense tracer uptake in kidneys, skeleton and urinary bladder (illustration 1e). Faint uptake in liver, spleen and salivary glands was also seen. Plotting of % of injected activity in source organs with respect to time (illustration 3), highest tracer localization was seen in skeletal system followed by liver, kidneys, spleen and salivary glands. In the skeletal target organ, there is an initial rapid uptake till 30 min followed by further gradual rise. Maximum tracer accumulation in skeletal system was found to be 18% of injected activity (IA) in one of the bronchial carcinoma patients with high burden of skeletal metastases.

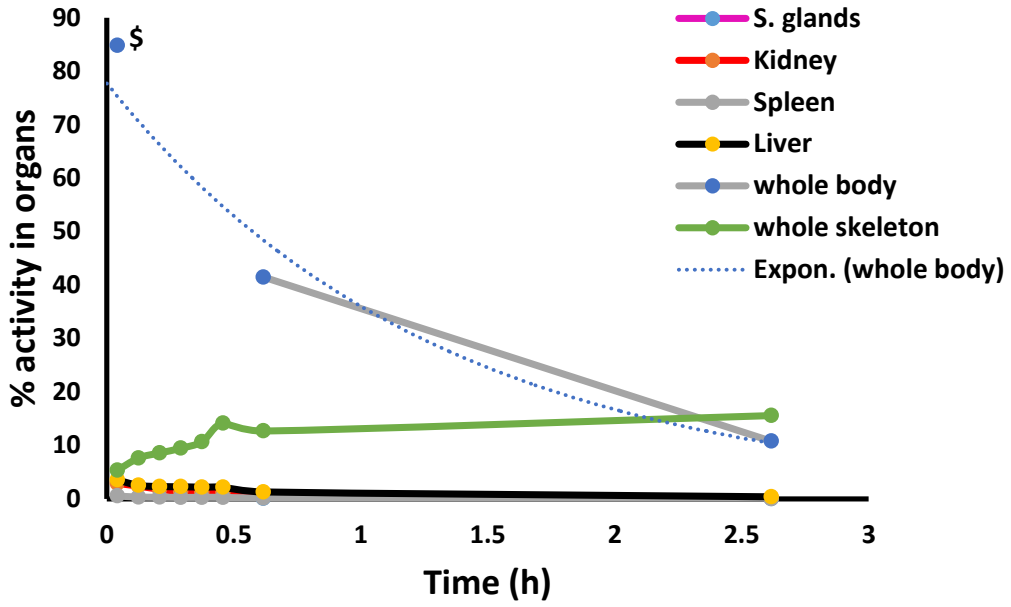

ill. 3: Change in % activity of [^{68}Ga]Ga-DOTA^{ZOL} in whole skeleton (without decay correction) and rest of source organs(without decay correction) and $(estimated initial activity) of patient no 2.

Fast tracer kinetics through kidneys with early peak uptake in renal parenchyma as early as 2.5 min followed by clearance with minimal activity in collecting system at 45 min p.i. and minimal to no residual activity at 2.5 h p.i. was appreciated both with visual analysis (illustration 3) as well as quantitative analysis (illustration 4). Almost 11 % of the injected activity remained in whole body at 2.5 h showing 89 % renal excretion.

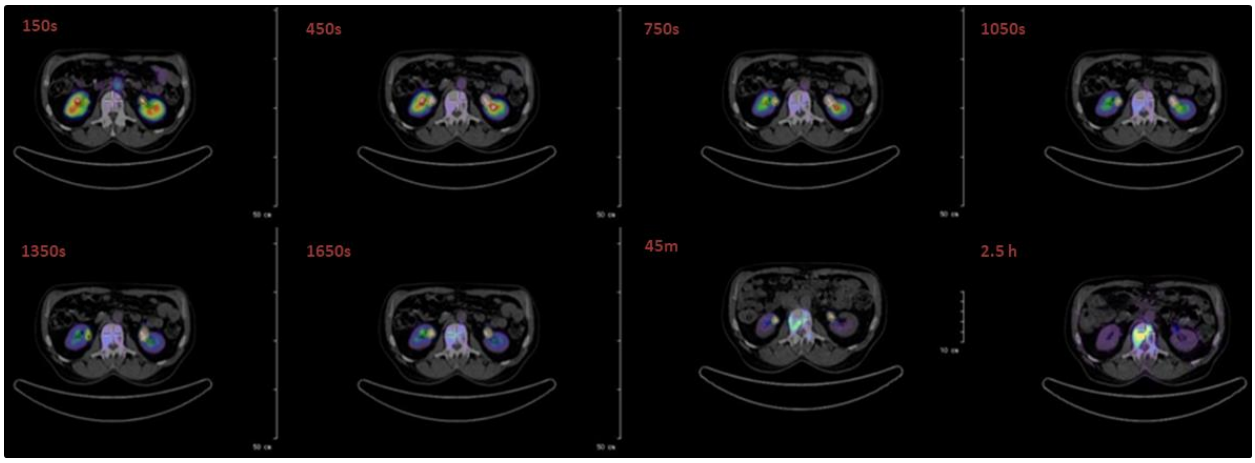

ill. 4: [^{68}Ga]Ga-DOTA^{ZOL} kinetics through kidneys in dynamic (150 s, 450 s, 750 s, 1050 s, 1350 s, 1650 s) and static images (45 min and 2.5 h). Patient no 3

Good bone to soft tissue and metastatic lesion to normal bone uptake was visualized at 45 min p.i.. which increased at 2.5 p.i Further comparison of mean SUV based skeletal to soft tissue ratio was found to be 7.36 and 12.96 at 45 min p.i. (illustration 5b) that increased to 15.03 and 28.82 at 2.5 h p.i. (illustration 5c) for two representative lesions in comparison to 4.81 and 3.30 on previous [^{68}Ga]Ga-PSMA-617 (illustration 5a) in patient with mCRPC. Lesion to normal bone ratio for these lesions was found to be 7.53 and 12.95 at 45 min and 6.79 and 13.01 at 2.5 h p.i.. on PET/CT images of [^{68}Ga]Ga-DOTA^{ZOL} in comparison to 7.5 and 5.14 respectively on [^{68}Ga]Ga-PSMA-617 image. The number of lesions were also found higher on [^{68}Ga]Ga-DOTA^{ZOL} as compared to [^{68}Ga]Ga-PSMA-617 in mCRPC patient.

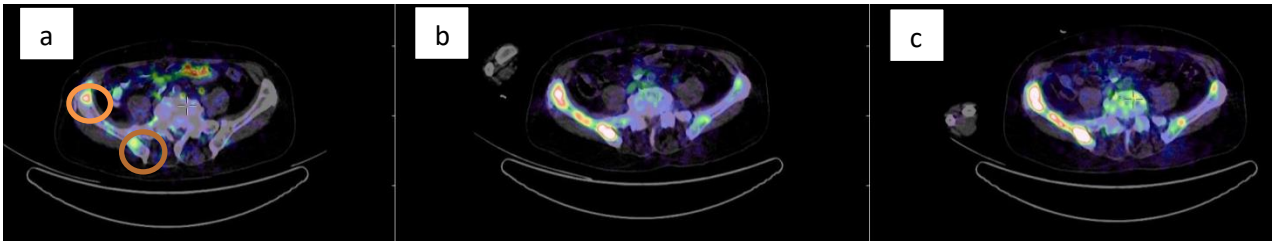

ill. 5: Uptake in two metastatic lesions on (a) [^{68}Ga]Ga-PSMA-617, (b) [^{68}Ga]Ga-DOTA^{ZOL} at 45 min p.i.. and (c) [^{68}Ga]Ga-DOTA^{ZOL} at 2.5 h p.i.. showing higher and progressive uptake with [^{68}Ga]Ga-DOTA^{ZOL} as a result of enhanced lesion to normal bone uptake. Patient no 1

Uptake in lesions and the apparent number of lesions were also found higher on visual comparison of [^{68}Ga]Ga-DOTA^{ZOL} with [^{18}F]FDG in bronchial carcinoma patients (illustration 6) and [^{99m}Tc]Tc-MDP bone scan in the female patient (illustration 7). SUV max in lesion was also found higher on [^{68}Ga]Ga-DOTA^{ZOL} (15.24 g/ml) as compared to [^{18}F]FDG PET/CT images (5.95 g/ml) in bronchial carcinoma patients.

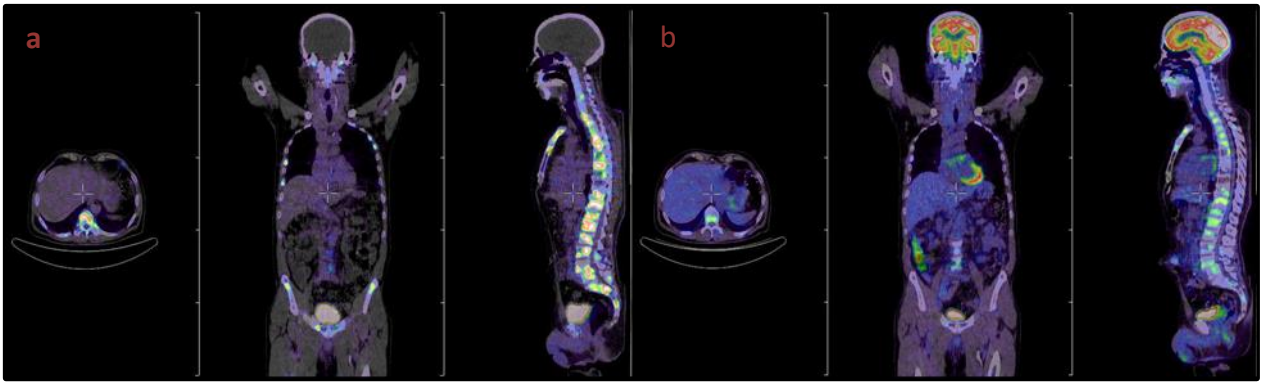

ill. 6: Comparison of PET/CT images of (a) [^{68}Ga]Ga-DOTA^{ZOL} with (b) [^{18}F]FDG in patient of skeletal metastases secondary to bronchial carcinoma. Patient no 4

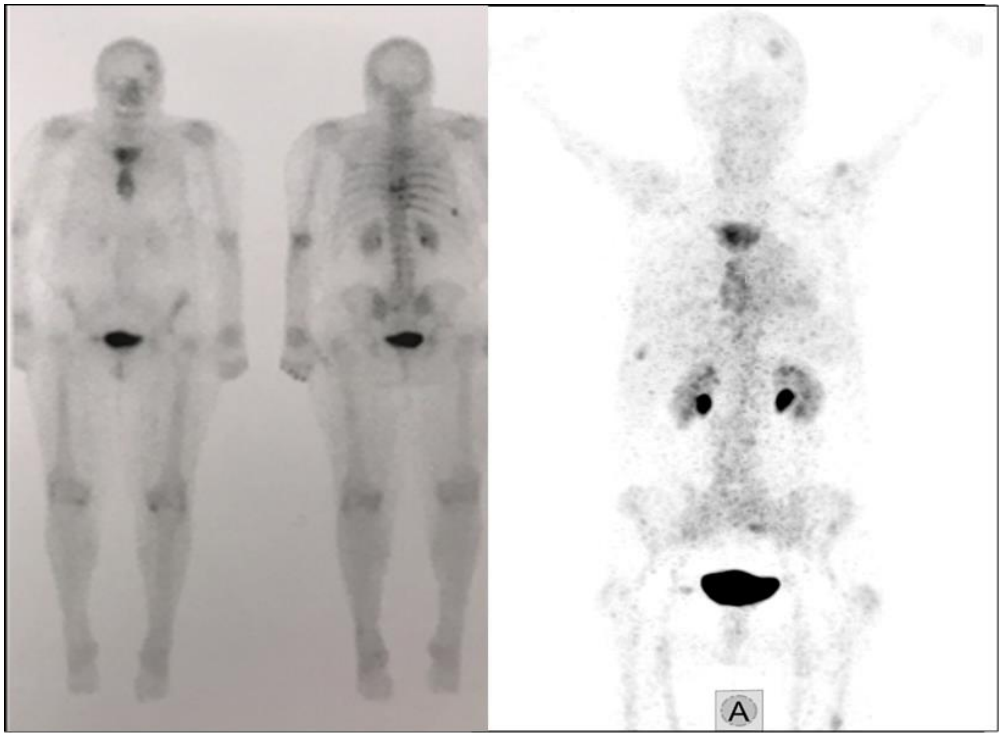

ill 7: Comparison of [^{99m}Tc]Tc-MDP with [^{68}Ga]Ga-DOTA^{ZOL} in patient of skeletal metastases secondary to breast carcinoma. Patient no 3

3.1.2 Dosimetric analysis for normal organs

Residence times (MBq-h/MBq) for source organs (table 8) were found highest for remainder of body followed by urinary bladder, cortical and trabecular bone, liver, red marrow, kidneys, spleen and salivary glands.

Organs	PT 1	PT 2	PT 3	PT 4	PT 5	mean	± SD
S. glands	0.004	0.002	0.001	0.001	0.001	0.002	0.001
Kidney	0.024	0.024	0.020	0.018	0.016	0.021	0.003
Spleen	0.005	0.004	0.008	0.004	0.006	0.005	0.001
Liver	0.057	0.034	0.052	0.028	0.032	0.040	0.012
Red marrow	0.034	0.038	0.053	0.039	0.058	0.042	0.009
Trabecular bone	0.148	0.117	0.116	0.225	0.150	0.127	0.041
Cortical bone	0.148	0.117	0.116	0.225	0.150	0.127	0.041
Urinary bladder	0.172	0.191	0.160	0.534	0.496	0.174	0.177
Remainder of body	0.392	0.468	0.213	0.251	0.377	0.358	0.095

Table 8: Residence time (MBq-h/MBq) in source organs with [^{68}Ga]Ga-DOTA^{ZOL}

Organ absorbed doses as well as effective dose according to ICRP103 (table 9) clearly describe that the urinary bladder was the critical organ as it received the highest absorbed dose of 0.368 mSv/MBq (range: 0.203-0.609 mSv/MBq) as kidneys were found to be the only route of its excretion. Osteogenic cells received dose of 0.040 mSv/ MBq followed by kidneys (0.031 mSv/MBq), red marrow (0.027 mSv/MBq), spleen (0.018 mSv/MBq), liver (0.013 mSv/ MBq) and salivary glands (0.011 mSv/MBq). Effective dose was calculated to be 2.61mSv from 150 MBq injected dose.

	PT 1	PT 2	PT 3	PT4	PT5	Mean	SD
Organs							
Adrenals	0.009	0.007	0.010	0.006	0.007	0.008	0.002
Brain	0.004	0.002	0.003	0.003	0.004	0.003	0.001
Breast			0.003			0.003	
Esophagus	0.005	0.002	0.004	0.003	0.004	0.004	0.001
Eyes	0.004	0.002	0.003	0.003	0.004	0.003	0.001
Gall bladder wall	0.007	0.004	0.005	0.004	0.005	0.005	0.001
Left colon	0.005	0.003	0.005	0.004	0.005	0.004	0.001
Small intestine	0.006	0.003	0.005	0.006	0.007	0.005	0.001
Stomach wall	0.005	0.002	0.004	0.003	0.004	0.004	0.001
Right colon	0.005	0.003	0.004	0.004	0.005	0.004	0.001
Rectum	0.008	0.006	0.011	0.013	0.014	0.011	0.003
Heart Wall	0.005	0.002	0.003	0.003	0.004	0.004	0.001
Kidneys	0.037	0.037	0.035	0.025	0.024	0.031	0.007
Liver	0.018	0.011	0.020	0.008	0.010	0.013	0.005
Lungs	0.005	0.002	0.004	0.003	0.004	0.003	0.001
Ovaries			0.007			0.007	
Pancreas	0.005	0.003	0.005	0.003	0.005	0.004	0.001
Prostate	0.010	0.008		0.017	0.018	0.009	0.001
Salivary glands	0.022	0.011	0.007	0.005	0.007	0.010	0.007
Red marrow	0.027	0.022	0.030	0.029	0.028	0.027	0.003
Osteogenic cells	0.042	0.034	0.035	0.049	0.041	0.040	0.006
Spleen	0.017	0.013	0.029	0.013	0.018	0.018	0.007
Testes	0.005	0.003		0.006	0.007	0.004	0.001
Thymus	0.004	0.002	0.003	0.003	0.004	0.003	0.001
Thyroid	0.004	0.002	0.003	0.003	0.004	0.003	0.001
Urinary bladder wall	0.203	0.222	0.235	0.609	0.572	0.368	0.204
Uterus			0.011			0.011	
Total Body	0.008	0.006	0.008	0.007	0.007	0.007	0.001
Effective dose from 150 MBq				2.61 mSv			

Table 9: Organ absorbed doses (mSv/MBq) and effective dose (mSv) from [^{68}Ga]Ga-DOTA^{ZOL}

3.2 [^{177}Lu]Lu-DOTA^{ZOL}

3.2.1 Qualitative analysis

Analysis of biodistribution of [^{177}Lu]Lu-DOTA^{ZOL} in serial images of two patients of bronchial carcinoma and two patients of prostate carcinoma with skeletal metastases revealed that at 20 min p.i. most of the activity was in soft tissue with highest uptake in

urinary bladder followed by kidneys with minimal accumulation in the skeleton. The kidneys showed a rapid decrease in activity at 3 h with minimum to no uptake after 24 h p.i. along with increasing intense uptake in the skeletal system from 3 h onwards. Blood and soft tissue clearance and lesion to normal bone contrast increased in later images up to 168 h. In this small patient study, we observed fast uptake and clearance kinetics of kidneys in patients with bronchial carcinoma (illustration 1a-d) as compared to mCRPC patient (illustration 8), which resulted in better skeletal to soft tissue contrast as early as 3 h p.i. in the bronchial carcinoma patient as compared to 24 h p.i. in mCRPC patient.

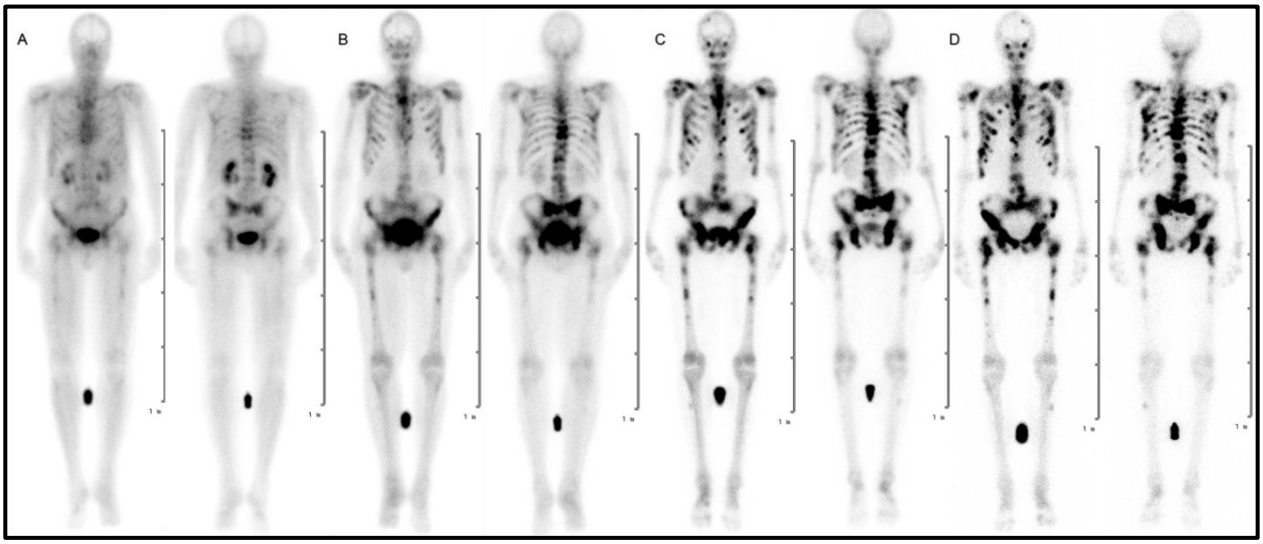

ill. 8: Planar scintigraphy (anterior and posterior views) after therapeutic application of [^{177}Lu]Lu-DOTA^{ZOL} at (a) 20 min, (b) 3 h, (c) 24 h, (d) 168 h in a patient with bone metastases secondary to prostate cancer (patient no 1)

3.2.2 Dosimetric analysis:

Mean residence times (MBq-h/MBq) (Table 10) was found to be highest in trabecular and cortical bone (31.9 h) followed by remainder of the body (11.7 h), kidneys (1.84 h), urinary bladder (1.52 h) and bone marrow (0.03 h). In patient no 1, residence times for the skeletal system and the kidney were lower as compared to the other patients.

	[^{177}Lu]Lu-DOTA^{zOL}					
Organs	**PT1**	**PT2**	**PT3**	**PT4**	**mean**	**± SD**
Kidneys	0.96	2.01	2.43	1.96	1.84	0.63
Trabecular bone	27.45	34.95	33.45	31.85	31.93	3.24
Cortical bone	27.45	34.95	33.45	31.85	31.93	3.24
Red marrow	0.01	0.03	0.04	0.03	0.03	0.01
Urinary bladder contents	1.59	1.48	1.51	1.50	1.52	0.05
Remainder of body	0.23	44.06	0.93	1.40	11.65	21.61
Whole body	56.10	116.00	70.30	67.10	77.38	26.46

Table 10: Residence times (MBq-h/MBq) of [^{177} Lu]Lu-DOTA^{ZOL}

Mean organ absorbed doses (Table 11) were found highest (3.33 ± 0.35 mSv/MBq) for osteogenic cells, followed by kidneys (0.49 ± 0.16 mSv/MBq), red marrow (0.461 ± 0.064 mSv/MBq) and urinary bladder wall (0.322 ± 0.022 mSv/MBq). Kidney and osteogenic cell absorbed doses were lowest in patient no 1. The mean total body dose was 0.092 ± 0.033 mSv/MBq.

	PT1	PT2	PT3	PT4	mean	±SD
Organs						
Adrenals	0.010	0.069	0.016	0.015	0.027	0.028
Brain	0.007	0.061	0.009	0.009	0.021	0.027
Esophagus	0.004	0.060	0.006	0.006	0.019	0.027
Eyes	0.007	0.061	0.009	0.009	0.021	0.027
Gall bladder wall	0.003	0.060	0.005	0.005	0.018	0.028
Left colon	0.005	0.062	0.007	0.007	0.020	0.028
Small intestine	0.004	0.061	0.006	0.006	0.019	0.028
Stomach wall	0.003	0.058	0.004	0.004	0.017	0.027
Right colon	0.003	0.060	0.005	0.005	0.018	0.028
Rectum	0.006	0.062	0.007	0.007	0.021	0.028
Heart wall	0.003	0.059	0.005	0.005	0.018	0.027
Kidneys	0.263	0.555	0.632	0.511	0.490	0.160
Liver	0.003	0.059	0.005	0.005	0.018	0.027
Lungs	0.004	0.059	0.005	0.006	0.019	0.027
Pancreas	0.004	0.061	0.006	0.006	0.019	0.028
Prostate	0.005	0.060	0.006	0.006	0.019	0.027
Salivary glands	0.004	0.060	0.006	0.006	0.019	0.027
Red marrow	0.402	0.551	0.456	0.434	0.461	0.064
Osteogenic cells	2.940	3.770	3.330	3.170	3.300	0.350
Spleen	0.004	0.060	0.006	0.006	0.019	0.027
Testes	0.003	0.057	0.004	0.004	0.017	0.027
Thymus	0.003	0.058	0.004	0.005	0.017	0.027
Thyroid	0.004	0.060	0.006	0.006	0.019	0.027
Urinary bladder wall	0.333	0.364	0.316	0.316	0.332	0.023
Total body	0.069	0.142	0.081	0.077	0.092	0.034

Table 11: Organ absorbed doses (mSv/MBq) of [^{177}Lu]Lu-DOTA^{ZOL}

3.3 Post-therapeutic organ absorbed doses for [^{177}Lu]Lu-DOTA^{ZOL} derived from mathematical extrapolation of [^{68}Ga]Ga-DOTA^{ZOL} Pharmacokinetics

Residence times (table 12) from integration of source organ activities obtained from mathematical extrapolation of [^{68}Ga]Ga-DOTA^{ZOL} data for [^{177}Lu]Lu-DOTA^{ZOL} are given below. Residence times for all source organs were found to be low as compared to same calculated from therapeutic doses of [^{177}Lu]Lu-DOTA^{ZOL} mentioned above.

Organs	PT1	PT2	PT3	PT4	PT 5	mean	± SD
Kidneys	0.06	0.04	0.05	0.04	0.04	0.05	0.01
Trabecular bone	0.29	1.77	0.26	22.40	19.00	8.74	11.00
Cortical bone	0.29	1.77	0.26	22.40	19.00	8.75	11.00
Red marrow	0.33	0.28	0.16	3.17	0.25	0.84	1.30
Urinary bladder contents	0.48	1.48	1.06	4.44	15.10	4.51	6.11
Remainder of Body	69.63	56.00	56.00	22.50	54.00	51.63	17.44

Table 12: Residence times for [^{177}Lu]Lu-DOTA^{ZOL} computed from [^{68}Ga]Ga-DOTA^{ZOL}

The organ absorbed doses for post [^{177}Lu]Lu-DOTA^{ZOL} therapy from extrapolation of pharmacokinetic analysis of [^{68}Ga]Ga-DOTA^{ZOL} (table 13) showed that osteogenic cells with 1.037 mSv/MBq received highest absorbed dose followed by urinary bladder (1.021 mSv/MBq) and bone marrow (0.238 mSv/MBq). Kidneys absorbed dose was found to be 0.020 mSv/MBq). As compared to the organ absorbed doses determined with therapeutic doses of [^{177}Lu]Lu-DOTA^{ZOL}, it was clearly seen that pre-therapeutic dosimetric analysis with [^{68}Ga]Ga-DOTA^{ZOL} computed lower organ absorbed doses. Moreover, similar to post [^{177}Lu]Lu-DOTA^{ZOL} therapy dosimetric analysis, osteogenic cells received highest absorbed dose however the computed values was three times less. Moreover red marrow and kidney doses were found two times and 24 times lower with [^{68}Ga]Ga-DOTA^{ZOL} extrapolation.

	PT1	PT2	PT3	PT4	PT5	mean	±SD
Organs							
Adrenals	0.090	0.072	0.089	0.035	0.073	0.072	0.022
Brain	0.088	0.071	0.086	0.034	0.073	0.070	0.022
			0.085				
Esophagus	0.089	0.072	0.086	0.033	0.072	0.070	0.023
Eyes	0.088	0.071	0.086	0.034	0.073	0.070	0.022
Gall bladder wall	0.090	0.073	0.090	0.032	0.072	0.071	0.024
Left colon	0.092	0.074	0.090	0.034	0.075	0.073	0.023
Small intestine	0.092	0.074	0.089	0.034	0.077	0.073	0.023
Stomach wall	0.090	0.073	0.089	0.031	0.072	0.071	0.024
Right colon	0.092	0.074	0.090	0.033	0.074	0.072	0.024
Rectum	0.092	0.075	0.092	0.038	0.088	0.077	0.023
Heart Wall	0.091	0.073	0.089	0.032	0.072	0.071	0.024
Kidneys	0.024	0.016	0.024	0.017	0.020	0.020	0.004
Liver	0.021	0.021	0.078	0.015	0.014	0.030	0.027
Lungs	0.089	0.072	0.088	0.032	0.072	0.071	0.023
Pancreas	0.092	0.074	0.091	0.033	0.074	0.073	0.024
Prostate	0.092	0.075	0.090	0.037	0.092	0.077	0.023
Salivary glands	0.186	0.141	0.082	0.043	0.086	0.108	0.056
Red marrow	0.171	0.093	0.080	0.493	0.353	0.238	0.179
Osteogenic cells	0.128	0.241	0.074	2.580	2.160	1.037	1.228
Spleen	0.024	0.017	0.028	0.015	0.023	0.021	0.005
Testes	0.089	0.072		0.032	0.075	0.067	0.024
Thymus	0.090	0.072	0.088	0.031	0.071	0.071	0.023
Thyroid	0.090	0.072	0.086	0.033	0.072	0.071	0.023
Urinary bladder wall	0.189	0.374	0.376	0.955	3.210	1.021	1.257
			0.092				
Total Body	0.094	0.079	0.091	0.096	0.137	0.099	0.022

Table 13: Post therapeutic organ absorbed doses for [^{177}Lu]Lu-DOTA^{ZOL} computed from [^{68}Ga]Ga-DOTA^{ZOL}

3.4 [^{44}Sc]Sc-PSMA-617:

3.4.1 Qualitative [^{44}Sc]Sc-PSMA-617 Distribution and Kinetics

Initial 30 min dynamic abdominal and three serial whole body PET/CT images (illustration 2) of patients administered with [^{44}Sc]Sc-PSMA-617 showed its physiological uptake in kidneys, liver, spleen, salivary glands, small intestine and urinary bladder which were selected as source organs for further dosimetric analysis. Very faint

uptake was also noticed in lacrimal glands with faint to absent uptake in nasal or oral mucosa. Pathological uptake was also observed in metastatic bone and soft tissue. Rapid blood clearance and excretion from kidneys created better tumor to soft tissue contrast.

Plotting % injected activity in source organs with time (illustration 9) revealed peak uptake in all source organs achieved before 1 h. Highest % injected activity was seen in liver followed by kidneys, spleen, salivary glands and small intestine. Rapid fall in activity in liver and other source organs was observed. The decrement in kidneys, small intestine and salivary glands was gradual with exception of increase in activity at 2 h in salivary glands and small intestine in only one patient.

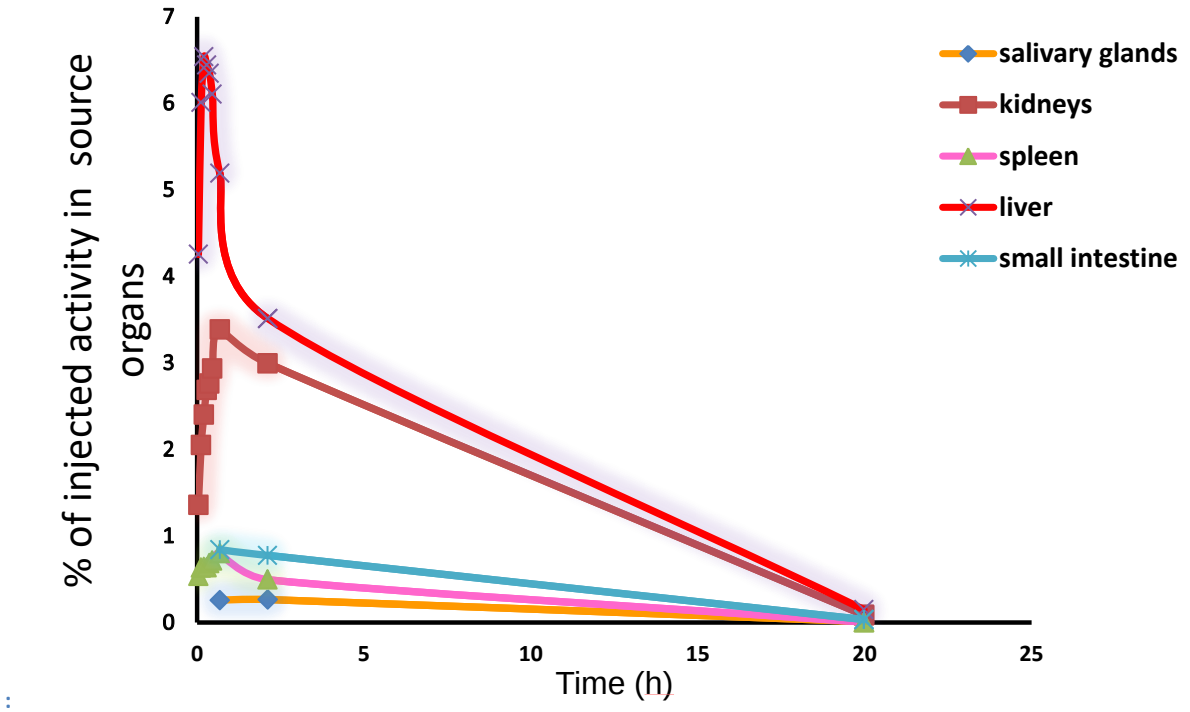

ill. 9: Time dependent changes of % injected activity in source organs

3.4.2 Dosimetry for Normal Organs

Residence times (MBq-h/MBq) of [^{44}Sc]Sc-PSMA-617 in source organs was highest in liver followed by kidneys, urinary bladder, bone marrow and rest of organs (table14)

PT No	PT1	PT2	PT3	PT4	PT5	mean	±SD
Organs							
Salivary glands	0.02	0.01	0.01	0.03	0.07	0.03	0.027
Kidneys	0.22	0.36	0.12	0.34	0.15	0.24	0.109
Liver	0.25	0.78	0.07	0.29	0.37	0.35	0.263
Spleen	0.08	0.09	0.02	0.05	0.09	0.07	0.031
Small intestine	0.02	0.04	0.02	0.07	0.08	0.05	0.029
Bone marrow	0.06	0.10	0.05	0.09	0.17	0.09	0.047
Urinary bladder contents	0.08	0.14	0.12	0.53	0.05	0.18	0.195
Remainder of body	2.93	1.11	1.45	1.86	1.76	1.82	0.684

Table 14: Residence times (MBq-h/MBq) of [^{44}Sc]Sc-PSMA-617 in source organs

Mean organ absorbed dose (mSv/ MBq) from diagnostic dose of [^{44}Sc]Sc-PSMA-617 (table 15) was found highest in the kidneys 0.319 mSv/ MBq (range: 0.180 to 0.488 mSv/ MBq) making it the critical organ followed by urinary bladder wall, spleen, salivary glands, liver and small intestine. Highest dose to kidneys were associated with the fact that they are the main route of excretion for PSMA-617. Bone marrow dose was found to be low and presented as organs with low toxicity risk while considering therapeutic application.

	PT 1	PT 2	PT 3	PT4	PT5	Mean	±SD
Organs							
Adrenals	0.079	0.112	0.042	0.092	0.056	0.076	0.028
Brain	0.027	0.011	0.015	0.018	0.015	0.017	0.006
Esophagus	0.035	0.027	0.019	0.027	0.022	0.026	0.006
Eyes	0.027	0.011	0.015	0.018	0.015	0.017	0.006
Gall bladder wall	0.051	0.073	0.024	0.047	0.040	0.047	0.018
Left colon	0.042	0.030	0.023	0.037	0.027	0.032	0.008
Small intestine	0.051	0.047	0.032	0.079	0.067	0.055	0.018
Stomach wall	0.040	0.031	0.021	0.031	0.025	0.030	0.007
Right colon	0.041	0.033	0.025	0.036	0.026	0.032	0.007
Rectum	0.038	0.023	0.026	0.048	0.022	0.031	0.011
Heart Wall	0.037	0.029	0.020	0.028	0.023	0.027	0.007
Kidneys	0.293	0.488	0.180	0.456	0.178	0.319	0.148
Liver	0.085	0.229	0.030	0.097	0.095	0.107	0.074
Lungs	0.033	0.024	0.018	0.025	0.020	0.024	0.006
Pancreas	0.043	0.037	0.023	0.037	0.029	0.034	0.008
Prostate	0.040	0.026	0.028	0.057	0.021	0.034	0.014
Salivary glands	0.097	0.035	0.052	0.116	0.253	0.111	0.086
Red Marrow	0.036	0.033	0.025	0.037	0.034	0.033	0.005
Osteogenic cells	0.030	0.023	0.019	0.028	0.026	0.025	0.004
Spleen	0.235	0.248	0.064	0.163	0.216	0.185	0.075
Testes	0.030	0.014	0.018	0.027	0.015	0.021	0.007
Thymus	0.032	0.018	0.018	0.022	0.018	0.022	0.006
Thyroid	0.031	0.015	0.017	0.021	0.017	0.020	0.006
Urinary Bladder wall	0.121	0.172	0.155	0.605	0.068	0.224	0.216
Total Body	0.034	0.023	0.019	0.284	0.020	0.076	0. 116
Mean effective Dose	0.0389 mSv/MBq						
Effective dose from 50 MBq	1.94 mSv						
Effective dose from 62 MBq	2.41 mSv						

Table 15: Organ absorbed doses (mSv/MBq) of [^{44}Sc]Sc-PSMA-617

3.5 Post-therapeutic organ absorbed doses for [^{177}Lu]Lu-PSMA-617 derived from mathematical extrapolation of [^{44}Sc]Sc-PSMA-617 Pharmacokinetics

Extrapolated mean residence times (MBq-h/MBq) of [^{177}Lu]Lu-PSMA-617 (table 16) were highest in liver (4.46 h) followed by the kidneys (1.51 h), small intestine (0.63 h), bone marrow (0.52 h), urinary bladder (0.33 h), salivary glands (0.21 h) and spleen

(0.18 h). Residence times in remainder of body showed high variation among patients and was found highest in patient 1.

Patient No	PT1	PT2	PT3	PT4	PT5	mean	±SD
Organs							
Salivary glands	0.10	0.59	0.24	0.19	0.08	0.24	0.21
Kidneys	1.07	1.25	1.17	1.96	2.09	1.51	0.48
Liver	3.48	2.85	3.31	6.18	6.46	4.46	1.72
Spleen	0.28	0.19	0.09	0.15	0.20	0.18	0.07
Small Intestine	0.83	0.45	0.71	1.05	0.09	0.63	0.37
Bone marrow	0.08	0.66	0.06	0.12	1.67	0.52	0.69
Urinary bladder contents	0.23	0.25	0.18	0.90	0.08	0.33	0.32
Remainder of body	64.12	43.72	22.40	44.86	57.80	46.58	16.04

Table 16: Extrapolated residence times (MBq-h/MBq) of [^{177}Lu]Lu-PSMA-617

Individual and mean organ absorbed doses of [^{177}Lu]Lu-pSMA-617 extrapolated from [^{44}Sc]Sc-PSMA-617 (table 17) revealed kidneys as critical organs with highest mean organ absorbed dose (0.44 mSv/MBq), followed by the salivary glands (0.23 mSv/MBq), liver (0.22 mSv/MBq), small intestine (0.14 mSv/MBq), spleen and urinary bladder wall with 0.12 mSv/MBq each. Mean bone marrow absorbed dose was found to be 0.05 mSv/MBq and mean whole body dose was 0.08 mSv/MBq.

Patient No	PT 1	PT 2	PT 3	PT4	PT5	Mean	±SD
Organs							
Adrenals	0.04	0.06	0.04	0.07	0.06	0.05	0.01
Brain	0.08	0.05	0.03	0.05	0.05	0.05	0.02
Esophagus	0.10	0.05	0.03	0.05	0.05	0.06	0.02
Eyes	0.08	0.05	0.03	0.05	0.05	0.05	0.02
Gall bladder wall	0.13	0.06	0.04	0.06	0.06	0.07	0.03
Left colon	0.13	0.05	0.03	0.06	0.06	0.07	0.04
Small intestine	0.20	0.11	0.12	0.19	0.07	0.14	0.06
Stomach wall	0.12	0.05	0.03	0.06	0.05	0.06	0.03
Right colon	0.10	0.05	0.03	0.06	0.06	0.06	0.03
Rectum	0.08	0.05	0.03	0.06	0.05	0.06	0.02
Heart Wall	0.09	0.05	0.03	0.06	0.06	0.06	0.02
Kidneys	0.54	0.33	0.34	0.52	0.47	0.44	0.10
Liver	0.24	0.14	0.17	0.29	0.26	0.22	0.06
Lungs	0.09	0.05	0.03	0.05	0.05	0.06	0.02
Pancreas	0.13	0.05	0.03	0.06	0.06	0.07	0.04
Prostate	0.08	0.05	0.03	0.06	0.05	0.06	0.02
Salivary glands	0.11	0.55	0.25	0.18	0.07	0.23	0.19
Red Marrow	0.07	0.06	0.03	0.04	0.04	0.05	0.02
Osteogenic cells	0.06	0.04	0.02	0.03	0.03	0.04	0.02
Spleen	0.26	0.11	0.06	0.09	0.10	0.12	0.08
Testes	0.08	0.05	0.03	0.05	0.05	0.05	0.02
Thymus	0.08	0.05	0.03	0.05	0.05	0.05	0.02
Thyroid	0.08	0.05	0.03	0.05	0.05	0.05	0.02
Urinary Bladder wall	0.13	0.10	0.07	0.24	0.07	0.12	0.07
Total Body	0.17	0.06	0.04	0.06	0.06	0.08	0.05

Table 17: Extrapolated organ absorbed doses of [^{177}Lu]Lu-PSMA-617

In order to calculate maximum permissible activity of [^{177}Lu]Lu-PSMA-617 (table 18) that can be administered in each patient with respect to dose limits derived from external beam radiotherapy(EBRT) i.e. kidneys (23 Gy), bone marrow(2 Gy), whole body(2 Gy), salivary glands(25 Gy), liver(30 Gy), small intestine(40 Gy) and urinary bladder(60 Gy), normal tissue dose limit of these organs was divided by corresponding organ absorbed doses in each patient.

Patient No	PT 1	PT 2	PT 3	PT4	PT5	Mean
Organs						
Small intestine	198.02	366.97	336.13	216.22	611.62	285.00
Kidneys	42.36	68.86	67.65	44.06	49.15	52.11
Liver	126.58	220.59	176.47	103.09	117.19	137.61
Salivary glands	235.85	45.45	102.04	136.61	379.64	108.71
Red Marrow	29.07	32.52	74.07	46.95	56.66	42.52
Urinary Bladder wall	472.44	576.92	874.64	250.00	865.80	492.69
Total Body	11.76	34.60	54.20	31.55	33.22	25.75

Table 18: Predicted maximum feasible activity (GBq) in individual patients considering toxicity limits for organs with EBRT

In patient 1 and 2, maximum permissible activity was determined by the red marrow absorbed dose and in patient 3, 4 and 5 the kidney absorbed dose was the limiting factor. In case of patient 1, renal dose was also high, resulting in a high cumulative dose to the whole body further limiting the maximum permissible activity. Toxicity limits for the salivary glands, small intestine and urinary bladder were found to exert no influence in this context.

4 Discussion

With rapid advancements in development of new radiopharmaceuticals, nuclear medicine has evolved from imaging of biological targets to targeted drug delivery against these specific targets. The combined use of radiopharmaceuticals designed for same molecular target for diagnosis and treatment with aim of patient-specific treatment has introduced concept of theranostics and personalized medicine in nuclear medicine. Radiation dosimetric analysis is an important aspect of theranostics that assesses safety and efficacy of radionuclide therapy as well as the safety of diagnostic radiopharmaceutical used as counter-part. At present, the most successful groups of isotopes for theranostics are ^{123}I/^{124}/I/ ^{131}I, ^{68}Ga/^{177}Lu and ^{111}In/^{86}Y/^{90}Y (Eberlein et al., 2017).

Several studies advocate that theranostic concept can be utilized for prediction of absorbed doses for therapeutic radionuclide. ^{124}/I/ ^{131}I pair has been successfully applied with this intent in differentiated thyroid carcinoma and prostate carcinoma (Erdi et al., 1999; Zechmann et al., 2014). Many new compounds other than octreotides e.g., PSMA, bisphosphonates, bombesin analogues have been labeled with ^{68}Ga for PET/ CT imaging and ^{177}Lu for therapy. Besides having different chemistry, the supposedly similar pharmacology has established use of ^{68}Ga labeled compounds for diagnosis and follow-up of disease. However, the theranostic use of short lived ^{68}Ga labeled compounds for prediction of absorbed doses for ^{177}Lu labeled compounds need to be assessed. The comparison of hypothetical uptake kinetics of ^{68}Ga with ^{177}Lu showed that it only covers the very early phase of pharmacology of analogue compound (Rösch et al., 2017) thus questioning its potential to assess accurate biokinetics and related areas under the time-activity curves for normal organs and tumor lesions. As physical half-life of diagnostic radionuclide seems to be an important consideration in predictive theranostic capability interest is geared for PET radionuclides with long half-life such as ^{44}Sc having half-life of 3.9 h to determine uptake kinetics for structurally similar ^{177}Lu labeled therapeutic compounds.

MIRD schema proposed by Medical Internal Radiation Dose (MIRD) committee of the Society of Nuclear Medicine provides the guidelines for appropriate data selection

for kinetic analysis of radionuclides used for diagnostic as well as therapeutic purposes. The MIRD formula to be applied at organ and voxel level for normal organs and tumor lesions respectively has been extensively explained in MIRD pamphlet no 21 and 17 respectively. The advancement in radiation dosimetric analysis of radionuclides suggests use of normal tissue complications probability (NCTP) and tumor control probability (TCP) in correlation with dose volume histograms for normal organs and tumor lesions for optimal treatment dose determination.

In this research work we have evaluated biodistribution and safety of [^{68}Ga]Ga-DOTA^{ZOL} and [^{177}Lu]Lu-DOTA^{ZOL} as new theranostic bisphosphonates for metastatic skeletal disease along with predictive theranostic potential of [^{68}Ga]Ga-DOTA^{ZOL} for [^{177}Lu]Lu-DOTA^{ZOL}. Also in view of better potential of ^{44}Sc with long half-life for theranostics, biodistribution, dosimetric analysis and of [^{44}Sc]Sc-PSMA-617 as new diagnostic radionuclide for mCRPC patients along with determination of post therapeutic absorbed doses for [^{177}Lu]Lu-PSMA-617 from its pharmacokinetic analysis has been assessed. The three radiopharmaceuticals are discussed one by one

4.1 Biodistribution and dosimetric analysis of [^{68}Ga]Ga-DOTA^{ZOL}

Bisphosphonates are analogues of naturally occurring pyrophosphates that are resistant to chemical or enzymatic hydrolysis. Their antiresorptive effect is mediated by high affinity for bone mineral and inhibitory effects on osteoclasts. Since long, radiolabeled bisphosphonates have been in use for imaging and bone pain palliation of metastatic skeletal disease. Use of macro cyclic chelators DOTA and NOTA for labeling bisphosphonates with trivalent metals like ^{68}Ga for diagnosis and ^{177}Lu for therapy resulted in development of labeled BPAPD, DOTA^{ZOL} and NO2AP^{BP} respectively. Among these NO2AP^{BP} is considered the most potent ^{68}Ga labeled bisphosphonate. However, its therapeutic counter- part labeled with ^{177}Lu was found inferior to [^{177}Lu]Lu-BPAPD. At present, [^{68}Ga]Ga-NO2AP^{BP} and [^{177}Lu]Lu-BPAMD are considered as theranostic pair for bone pain palliation. Preclinical animal and *in vitro* studies have proposed [^{68}Ga]Ga-DOTA^{ZOL} in combination with [^{177}Lu]Lu-DOTA^{ZOL} and [^{225}Ac]Ac-DOTA^{ZOL} as new theranostic bisphosphonate for metastatic skeletal disease patients.

Hence, necessitates evaluation of biodistribution and dosimetric analysis of [^{68}Ga]Ga-DOTA^{ZOL}.

The biodistribution and dosimetric analysis of [^{68}Ga]Ga-DOTA^{ZOL} was studied for first time in humans. The patients of bronchial carcinoma, mCRPC and breast carcinoma with metastatic skeletal disease were injected with [^{68}Ga]Ga-DOTA$^{ZOL.}$. Like other bis-phosphonates and bone seeking agents, kidneys were found to be the route of excretion. Fast tracer kinetics through kidneys (illustration 3 and 4) was seen resulting in whole body activity to decease to almost 11 % till 2.5 h p.i.. Skeletal system showed initial rapid accumulation followed by gradual rise. Initial uptake in liver, spleen and salivary glands was also seen followed by sharp decline.

Soft tissue and blood activity decreased with time and resulted in enhanced bone uptake and increased metastatic lesion to bone ratio (illustration 5) which is consistent with results of other ^{68}Ga-bisphosphonate agents and [^{18}F]NaF (Meckel *et al*, 2017; Pfannkuchen *et al*, 2017). PET/CT images of [^{68}Ga]Ga-DOTA^{ZOL} could be compared to previous [^{68}Ga]Ga-PSMA-617 and [^{18}F]FDG PET/CT images in the male patients and a [^{99m}Tc]Tc-MDP bone scan enrolled in this study. Here, the uptake of [^{68}Ga]Ga-DOTA^{ZOL} was 2.56 times higher than [^{18}F]FDG in bronchial carcinoma patient . Apparent number of lesions were also found more with [^{68}Ga]Ga-DOTA^{ZOL} as compared to [^{68}Ga]Ga-PSMA-617 (illustration 5), [^{18}F]FDG in bronchial carcinoma (illustration. 6) and [^{99m}Tc]Tc-MDP in breast carcinoma patient (illustration 7].

Compared with [^{68}Ga]Ga-PSMA-617, the qualitative analysis of [^{68}Ga]Ga-DOTA^{ZOL} showed better uptake in skeleton with higher skeleton to soft tissue and metastatic lesion to normal bone ratio (illustration 5). This finding is consistent with in vivo biodistribution analysis of [^{68}Ga]Ga-DOTA^{ZOL} in one patient of prostate cancer (Pfannkuchen et al., 2017).

As [^{18}F]NaF is the bone seeking radiopharmaceutical with highest sensitivity and specificity for metastatic skeletal disease, the dosimetric analysis of [^{68}Ga]Ga-DOTA^{ZOL} was compared with [^{18}F]NaF. Residence times (table 8) for remainder of body of [^{68}Ga]Ga-DOTA^{ZOL} (0.358 h) was found comparable to that of [^{18}F]NaF 0.33 reported in ICRP 106 report (ICRP, 2008). Urinary bladder residence time (0.174 h) of [^{68}Ga]Ga-DOTA^{ZOL} was found to be less than that of [^{18}F]NaF (0.19 and 0.29 h), however the residence time for kidneys was found to be higher (0.022 h) as compared to [^{18}F]NaF

(0.01 h). This could be explained by the fact that [^{68}Ga]Ga-DOTA^{ZOL} has shown 89 % of renal excretion over a period of 2.5 h as compared to 15% and 50% in case of [^{18}F]NaF (ICRP, 2008; Kurdziel et al., 2012;) The residence time of [^{68}Ga]Ga-DOTA^{ZOL} in trabecular and cortical bone was found to be 0.127 with 50 % weightage given to both. The residence time in bone components as well as bone marrow were lower as compared to [^{18}F]NaF. It might be a result of lower half-life of ^{68}Ga as compared to ^{18}F as well as the difference of osteogenic tumor load in patients evaluated by Kurdziel et al and the current study. Residence times for liver and spleen were found higher than [^{18}F]NaF. The uptake of free/ unbound ^{68}Ga can be responsible for prolonged residence times in these organs.

[^{68}Ga]Ga-DOTA^{ZOL} like other bone seeking agents was found to be characterized with delivering highest radiation absorbed dose to urinary bladder, followed by osteogenic cells, red marrow and kidneys (table 9). This finding is comparable with dosimetric analysis of [^{18}F]NaF (ICRP, 2008; Kurdziel et al., 2012). Kidney being its physiological route of excretion results in highest dose to urinary bladder. The doses delivered to urinary bladder and kidneys were 2.4 times higher and radiation absorbed doses to osteogenic tissue and red marrow were lower as compared to [^{18}F]NaF (ICRP, 2008; Kurdziel et al., 2012). Mean effective dose and total effective dose were found to be 0.017 mSv/MBq and 2.61 mSv with [^{68}Ga]Ga-DOTA^{ZOL} comparable to 0.017 mSv/MBq and 1.88 – 3.15mSv with [^{18}F]NaF respectively (ICRP, 2008; Kurdziel et al., 2012).

As described earlier [^{68}Ga]Ga-NO2AP^{BP} is considered the most potent ^{68}Ga labeled bisphosphonates so dosimetric analysis of [^{68}Ga]Ga-DOTA^{ZOL} was compared with [^{68}Ga]Ga-NO2AP^{BP} (Passah et al., 2017). The comparison revealed high absorbed doses delivered to kidneys and urinary bladder, almost comparable absorbed doses to bone marrow and osteogenic cells, high total body absorbed dose and high effective dose equivalent which illustrates the superiority of [^{68}Ga]Ga-NO2AP$^{BP.}$ The difference of kidney and urinary bladder absorbed doses could be due to difference of collection of data points till 4 h for [^{68}Ga]Ga-NOTAP^{BP} in comparison to 2.5 h in current study. Further lack of detailed biodistribution analysis is also a limitation for comparing the results of the two studies. It was observed that the dosimetric results of [^{68}Ga]Ga-NO2AP^{BP} from

breast carcinoma patients (M:F; 1:4) were not comparable to results for the one female breast carcinoma patient (Pt 3) of the current study.

The resultant high urinary bladder and kidney absorbed doses from [^{68}Ga]Ga-DOTA^{ZOL} is consistent with other bone seeking agents. These doses can very easily be reduced by proper hydration and rapid diuresis. As compared to various ^{68}Ga labeled octreotide (Walker et al., 2013) and PSMA agents (Afshar-Oromieh et al., 2015; Herrmann et al., 2015), [^{68}Ga]Ga-DOTA^{ZOL} delivered lower kidney and higher urinary bladder absorbed doses along with lower mean effective dose.

Besides having 2.4 times high radiation exposure to kidneys and urinary bladder as compared to [^{18}F]NaF, possibility of treatments of bone metastases with [^{177}Lu]Lu-DOTA^{ZOL} and [^{225}Ac]Ac-DOTA^{ZOL} gives [^{68}Ga]Ga-DOTA^{ZOL} a clear advantage over other bone seeking diagnostic agents such as [^{18}F]Na-F and [^{99m}Tc]Tc-MDP. These initial results are encouraging and support the use of [^{68}Ga]Ga-DOTA^{ZOL} as imaging theranostic agent. However, prospective patient studies are required to explore its further potential for the treatment of bone metastases in different tumor entities.

4.2 Biodistribution and dosimetric analysis of [^{177}Lu]Lu-DOTA^{ZOL}

Zoledronate presents as an ideal candidate for labeling with the therapeutic radionuclide lutetium-177 for radionuclide therapy of bone metastases, as it shows high osteoclast and hydroxyl apatite binding (Meckel et al., 2017) and no *in vivo* biotransformation (Nikzad et al., 2013). Preclinical small animal studies using [^{177}Lu]Lu-DOTA^{ZOL} and [^{68}Ga]Ga-DOTA^{ZOL} showed comparable results, suggesting the two tracers as new theranostic pair for bone-targeted radionuclide therapy (Meckel et al., 2017). Moreover, [^{177}Lu]Lu-DOTA^{ZOL} has also been proposed the therapeutic arm with [^{68}Ga]Ga-NODAGA^{ZOL} (suggested better than [^{68}Ga]Ga-DOTA^{ZOL} in preclinical studies). Hence, biodistribution and dosimetric analysis of [^{177}Lu]Lu-DOTA^{ZOL} was explored in patients with skeletal metastases.

Extrapolation of dosimetric analysis of [^{177}Lu]Lu-DOTA^{ZOL} and [^{177}Lu]Lu-EDTMP from rats to humans revealed high kidney and trabecular bone absorbed doses as well as high trabecular bone to other organs absorbed dose ratios for [^{177}Lu]Lu-DOTA^{ZOL}(Yousefnia et al., 2015). The higher thermodynamic and kinetic stability, leading to high bone uptake with low soft tissue accumulation, suggests [^{177}Lu]Lu-

DOTA^{ZOL} to be a better therapeutic bisphosphonate compared to [^{177}Lu]Lu-EDTMP (Bergmann et al., 2016).

As phase I and II studies with [^{177}Lu]Lu-EDTMP for bone pain palliation under IAEA CRP project have shown encouraging results, therefore we have compared the biodistribution and dosimetric analysis of results of [^{177}Lu]Lu-DOTA^{ZOL} with [^{177}Lu]Lu-EDTMP.

Biodistribution of [^{177}Lu]Lu-DOTA^{ZOL} in humans (illustrations 1a-d & 8) was consistent with preclinical biodistribution studies in male Wistar rats (Meckel et al., 2017; Yousefnia et al., 2015). Highest accumulation in the skeleton with fast kidney uptake and clearance was seen. As the kidneys are the sole route of its excretion, the urinary bladder showed high uptake as well. Blood and soft tissue showed rapid clearance which resulted in good skeleton to soft tissue contrast. A rapid and biphasic blood clearance curve was found comparable to [^{177}Lu]Lu-EDTMP (Bal et al., 2015) . No uptake was seen in any other organ. Prominent uptake in the skeletal system in bronchial carcinoma patients was visualized at 3 h p.i. image in contrast to 24 h p.i. in mCRPC patients. The finding of best bone-to-soft tissue contrast at 24 h p.i. in mCRPC patients is consistent with similar observations with [^{177}Lu]Lu-EDTMP distribution in mCRPC patients (Bal et al., 2015; Balter et al., 2015; Sharma et al., 2017). To establish whether the early uptake in bronchial carcinoma patients is a patient dependent or tumor dependent finding and can be of any significance in relation to tumor lesion doses needs further large scale and tumor lesion dosimetry studies.

The source organs identified for dosimetric analysis included the kidneys, bone marrow, urinary bladder, skeletal system and the whole body. A biphasic kinetic behavior of [^{177}Lu]Lu-DOTA^{ZOL} was observed in all source organs and the whole body. Hence, biexponential curve fitting was used for residence time calculations. Residence time of [^{177}Lu]Lu-DOTA^{ZOL} (table 10) was highest in the skeleton similar to [^{177}Lu]Lu-EDTMP (Bal et al., 2015). Residence time for all source organs except the kidneys were lower in comparison to [^{177}Lu]Lu-EDTMP (Bal et al., 2015). The low number of patients and the different methodology used for determination of residence time in our current study might be causes for this difference. However, the ratio of skeletal-to-whole body residence time was higher for [^{177}Lu]Lu-DOTA^{ZOL} compared to [^{177}Lu]Lu-EDTMP (Bal et al., 2015).

We found lower mean organ absorbed doses (table 11) for osteogenic cells (3.33 ± 0.35 mSv/MBq) compared to 5.41 and 5.26 mSv/MBq reported for [^{177}Lu]Lu-EDTMP (illustration 4) (Bal et al., 2015; Sharma et al., 2017) as well as 4.04 mSv/MBq for [^{153}Sm]Sm-EDTMP(Sharma et al, 2017). The difference might be due to humerus (Bal et al., 2015) or femoral activity (Sharma et al., 2017) extrapolation for skeletal activity and residence time calculations for [^{177}Lu]Lu-EDTMP as compared to calculation of skeletal activity by deduction of percent kidney, blood and bladder activity from percent whole body activity in current study.

In our study we found a higher mean organ absorbed dose (table 11) for the kidneys (0.49 mSv/MBq) as compared to [^{177}Lu]Lu-EDTMP (0.04 and 0.06 mSv/MBq) (Bal et al., 2015; Sharma et al., 2017). In contrast to the use of the conjugate view method for kidney residence time calculation in our current study, Bal et al.(Bal et al., 2015) neglected kidney self-dose in absorbed dose determination and Sharma et al(Sharma et al., 2017) used a different methodology for calculation of percent injected doses in kidneys which resulted in lower kidney dose for [^{177}Lu]Lu-EDTMP. Hence, the kidney absorbed doses reported for [^{177}Lu]Lu-EDTMP cannot be compared with the results of [^{177}Lu]Lu-DOTA^{ZOL} in our current study. The mean organ absorbed dose to the urinary bladder wall (0.332 mSv/MBq) was found to be lower in our study as compared to [^{177}Lu]Lu-EDTMP (1.53 mSv/MBq) (Bal et al., 2015; Sharma et al., 2017). This difference could be due to use of Clouttier´s method with cumulative urinary calculation from whole body retention and 4 h voiding intervals in our current study as compared to collection of urine samples for residence time calculation in the [^{177}Lu]Lu-EDTMP studies.

[^{177}Lu]Lu-DOTA^{ZOL} resulted in a lower bone marrow absorbed dose compared to [^{177}Lu]Lu-EDTMP (Bal et al., 2015; Sharma et al., 2017) which in theory allows administration of higher therapeutic activities of [^{177}Lu]Lu-DOTA^{ZOL}. Based on a maximum permissible radiation absorbed dose to the bone marrow of 2Gy, the maximum tolerated dose for [^{177}Lu]Lu-DOTA^{ZOL} is estimated to be 3630-4980 MBq as compared to 2000–3250 MBq for [^{177}Lu]Lu-EDTMP (Bal et al, 2015). As a result, radiation absorbed dose of 11 to 16 Gy will be delivered to osteogenic cells by [^{177}Lu]Lu-DOTA^{ZOL} which is comparable to 10.1 to 17.6 Gy for [^{177}Lu]Lu-EDTMP. Using these

thresholds, the kidney absorbed dose remains well below the maximum permissible dose limit of 23 Gy.

As absorbed dose to kidneys is one of the important factors in radionuclide therapy using Lutetium-177 labeled radiopharmaceuticals, we found that [^{177}Lu]Lu-DOTA^{ZOL} delivers a lower (by a factor of 1.2 to 1.88) kidney dose in comparison to [^{177}Lu]Lu-PSMA-617 and [^{177}Lu]Lu-HBED-CC(Kabasakal et al., 2015; Scarpa et al., 2017). [^{177}Lu]Lu-DOTA^{ZOL} has been found to be a promising new therapeutic radiopharmaceutical for radionuclide therapy of bone metastases due to excellent skeletal uptake, a lower bone marrow dose than [^{177}Lu]Lu-EDTMP and a very low kidney dose. Further studies are warranted to evaluate the efficacy and safety of radionuclide therapy with [^{177}Lu]Lu-DOTA^{ZOL} in the clinical setting.

4.3 Predictive dosimetry with [^{68}Ga]Ga-DOTA^{ZOL} for [^{177}Lu]Lu-DOTA^{ZOL}

The residence times (table 12) and mean organ absorbed doses (table 13) for [^{177}Lu]Lu-DOTA^{ZOL} determined from extrapolation of pharmacokinetics of [^{68}Ga]Ga-DOTA^{ZOL} were found to be low as compared to same (table 10 and table 11) determined from post therapeutic dosimetric analysis of [^{177}Lu]Lu-DOTA^{ZOL}. As bone marrow absorbed dose appeared to be important for maximum tolerated dose of [^{177}Lu]Lu-DOTA^{ZOL}, it appeared that lower extrapolated bone marrow absorbed dose will result in computation of higher therapeutic doses. Moreover, it was seen that individual absorbed doses for normal organs in patient no 4 and 5 with bronchial carcinoma were correlating better to the post therapeutic absorbed doses as compared to patients of prostate and breast carcinoma patient 1,2 and 3 respectively but still presented with lower doses. It could be due to individual difference of kinetics in these patients. Thus it is concluded that [^{68}Ga]Ga-DOTA^{ZOL} should not be used for prospective dosimetric analysis of [^{177}Lu]Lu-DOTA^{ZOL}. This finding is consistent with the fact that short half-life of ^{68}Ga cannot monitor the kinetics of ^{177}Lu (Rösch et al., 2017).

4.4 Biodistribution and dosimetric analysis of [^{44}Sc]Sc-PSMA-617

PSMA-617 is a modified version of PSMA-11 that binds to the external domain of PSMA. Comparative biodistribution studies with PSMA-11 has revealed supremacy of

PSMA-617 due to high target binding and subsequent efficient internalization with in prostate carcinoma cells (Afshar-Oromieh et al., 2015). It has been labeled with gallium-68, lutetium-177, indium-111 and yttrium-90. Although, pre and post [^{177}Lu]Lu-PSMA-617 therapy, theranostic use of [^{68}Ga]Ga-PSMA-617 for patient selection and disease monitoring is widely used (Afshar-Oromieh et al., 2015; Baum and Kulkarni, 2012), the dosimetric analysis results in lower organ absorbed doses as compared to [^{177}Lu]Lu-PSMA-617. Moreover, it is believed that short half-life (1.13 h) of [^{68}Ga]Ga-PSMA-617 is not suitable to follow the pharmacokinetics of [^{177}Lu]Lu-PSMA having half-life of 6.9 h and cannot be used for prediction of post therapeutic dosimetric analysis of [^{177}Lu]Lu-PSMA and personalized dose determination.

Recently PSMA-617 has been labeled with long lived PET agents like scandium-44 using DOTA as a linking chelator. Preclinical (in vitro, in vivo) and clinical studies with scandium-44 labeled peptides and PSMA ligand for neuroendocrine tumors (Singh et al., 2017) and prostate carcinoma (Umbricht et al., 2017) respectively have proposed scandium-44 a better surrogate marker for lutetium-177 based therapies and probable better candidate for pre-therapeutic dosimetric analysis. In this study we evaluated its feasibility as new imaging theranostic radionuclide in mCRPC patients.

In this study we found the physiological uptake of [^{44}Sc]Sc-PSMA-617 in liver, kidneys, salivary glands, spleen, small intestine, urinary bladder (illustration 2 and 9) consistent with low level uptake in normal organs of PSMA described in literature (Afshar-Oromieh et al., 2013, 2015). Pathological uptake was seen in both skeletal and soft metastatic tissue. Kidneys were the major route of excretion with rapid peak uptake seen at 45 min and fast clearance showing minimal activity at 18 h concurrent with early uptake and fast clearance characteristic of PSMA-617. Probable toxicity of salivary glands proposed by A Afshar- Oromieh et al due to late trapping of [^{68}Ga]Ga-PSMA-617 in salivary glands was not observed in this study (Afshar-Oromieh et al., 2015). Increase in activity in 2 h image was observed in only one of the patients which later decreased to minimal activity at 19.5 h while rest of the patients showed peak uptake at 45 min followed by gradual decrease. The low probability of salivary gland toxicity depicted by kinetics of [^{44}Sc]Sc-PSMA-617 is consistent with dosimetry results of [^{68}Ga]Ga-PSMA-617(Afshar-Oromieh et al., 2015). Occurrence of transient xerostomia

or mild reversible xerostomia with [^{177}Lu]Lu-PSMA-617 as well as other lutetium-177 labeled PSMA therapies also supports that salivary glands toxicity should be of less concern in these patients (Ahmadzadehfar *et al*, 2016; Baum *et al*, 2016; Rahbar *et al*, 2016a, 2016b). Lacrimal glands showed faint uptake with no enhanced accumulation in later images, therefore we considered its activity with in remainder of body activity. Faint to negligible uptake in nasal mucosa was seen with [^{44}Sc]Sc-PSMA-617. The rapid initial uptake in liver and spleen followed by fast clearance as result of blood pool effect and its clearance from these organs is consistent with literature (Afshar-Oromieh et al., 2015)

Quantitative analysis revealed high total activity (illustration 9) and prolonged residence time in liver (table 14) followed by kidneys, spleen and other organs consistent with results of [^{68}Ga]Ga-PSMA-617 (Afshar-Oromieh et al., 2015). Residence time of source organs with [^{44}Sc]Sc-PSMA-617 were found to be higher than [^{68}Ga]Ga-PSMA-617. Long half-life of 3.9 h and ability to follow bio kinetics up to 19.5 h or more with [^{44}Sc]Sc-PSMA-617 account for the higher residence times as compared to [^{68}Ga]Ga-PSMA-617.

The organ absorbed doses (table 15) were highest in kidneys followed by urinary bladder wall, spleen, salivary glands, liver and small intestine. Kidneys with mean dose of 0.319 mSv/MBq (range: 0.178-0.488 mSv/MBq) were the organs at risk as is with the rest of small ligands based PSMA agents (Afshar-Oromieh et al., 2015). Urinary bladder wall with mean dose of 0.224 mSv/MBq was the second highest organ to receive dose owing to the kidneys being its physiological route of excretion. Salivary glands received a dose of 0.111 mSv/MBq which was higher than [^{68}Ga]Ga-PSMA-I&T but was not reported with [^{68}Ga]Ga-PSMA-617 besides showing a rise in mean SUV at later time points (Afshar-Oromieh et al., 2015). Bone marrow dose was found to be low consistent with previous dosimetric studies with gallium-68 labeled agents. Mean organ absorbed dose for bone marrow was found to be 0.033 mSv/MBq and ranged from 0.025 to 0.037. Low marrow dose suggests low risk of marrow toxicity with PSMA based therapies. However, the marrow toxicity can vary with burden of bone and marrow metastases in the patient as was found to be highest in patient no 1 with high tumor burden. Further, our results are concurrent with that of [^{68}Ga]Ga-PSMA-617 ,[^{68}Ga]Ga-PSMA-11 and [^{68}Ga]Ga-PSMA-HBED-CC with reference to high to low dose received by organs.

However, absorbed doses were found to be higher for [^{44}Sc]Sc-PSMA-617 than [^{68}Ga]Ga-PSMA-617, [^{68}Ga]Ga-PSMA-11, [^{68}Ga]Ga-PSMA-I&T but less than [^{124}I]I-PSMA (Pfob et al., 2016).

Comparison of organ absorbed doses of [^{44}Sc]Sc-PSMA-617 with pre and post therapeutic dosimetric results of [^{177}Lu]Lu-PSMA-617(Delker et al, 2016; Kabasakal et al., 2015; Okamoto et al., 2017) and comparison of doses with other gallium labeled PSMA agents also show that it is able to predict doses better than [^{68}Ga]Ga-PSMA-617(Afshar-Oromieh et al., 2013, 2015). However interpatient dosimetric comparison studies of [^{44}Sc]Sc-PSMA-617 with [^{177}Lu]Lu-PSMA-617 are warranted.

The mean effective dose of 0.0398 was found to be higher than [^{68}Ga]Ga-PSMA-617, [^{68}Ga]Ga-PSMA-11, [^{68}Ga]Ga-PSMA-I&T but less than [^{124}I]I-PSMA (Pfob et al., 2016). The total effective dose with usual dose administered (50MBq) of [^{44S}Sc]Sc-PSMA-617 was found to be 1.95mSv which was low as compared to rest of gallium-68 labeled PSMA agents as well [^{124}I]I-PSMA.

Hence [^{44S}Sc]Sc-PSMA-617 having possibility of delayed imaging, higher organ absorbed doses and effective dose less than other PSMA labeled imaging agents and a similar biodistribution to already known ^{68}Ga-PSMA ligands could be a better and safe agent for prediction of therapeutic dosimetry for [^{177}Lu]Lu-PSMA-617. The biodistribution and dosimetric analysis in this study has proved that early uptake kinetics reaching peak followed by clearance of PSMA-617 from source organs up to 19.5 h can easily be interpreted. A comparison of [^{44S}Sc]Sc-PSMA-617 kinetics of our study with kinetics of [^{177}Lu]Lu-PSMA-617 shown by Delker et al (Delker et al., 2016) as well as in vivo kinetics of [^{177}Lu]Lu-PSMA-617 in pre-clinical small animal studies followed for 24 h (Benešová et al., 2015) has shown comparable biodistribution with peak uptake as early as 1 h followed by gradual clearance till 24 h. Moreover, the protocol can be completed within 24 hours and most important of all can be incorporated in daily clinical routine. It is important to mention that individual pre-therapeutic dosimetric analysis with [^{44}Sc]Sc-PSMA-617 is not necessary for all patients, but for patients not responding to standard doses or having a high cumulative dose or having reduced renal function in the lab.

4.5 Predictive dosimetry with [^{44}Sc]Sc-PSMA-617 for [^{177}Lu]Lu-PSMA-617

The mean ± SD of extrapolated residence time (table 16) for [^{177}Lu]Lu-PSMA-617 for the remainder of the body in our study was 46.58 ±16.04 h (range: 22.4 -64.12 h), which is in line with the results of the study of L. Kabasakal et al, (mean ± SD 37.9 ± 14.6 h ; range: 24.6 – 62.0 h). We also observed that patient 1, who had renal insufficiency as well as extensive bone metastasis, exhibited the longest residence time, which is consistent with the observations of L. Kabasakal et al (Kabasakal et al, 2015).

The extrapolated mean organ absorbed doses for [^{177} Lu]Lu-PSMA-617in our study were comparable with other pre-therapeutic and post-therapeutic dosimetry results obtained with [^{177}Lu]Lu-PSMA-617 (Delker et al., 2016; Fendler et al., 2017; Kabasakal et al., 2015; Kratochwil et al., 2016; Kulkarni et al., 2016; Okamoto et al., 2017). However, we observed a lower mean absorbed dose in the kidneys, compared to previous studies. This might be explained by the analysis of 3D PET/CT activity distribution in the kidneys, as compared to 2D planar gamma camera-based distribution measurement, which has inherent potential of over-estimation of kidney dose owing to activity contribution from overlapping organs. On the other hand, we observed a higher mean organ absorbed doses in whole body as compared to previous studies. This difference is mainly caused by the high residence time in the remainder of body in patient 1. The mean organ absorbed doses in the remaining organs were comparable to the values observed by previous studies.

Pre-therapeutic dosimetry aims at improving and tailoring dose delivery to tumor lesions while maintaining safety and avoiding toxicity to normal organs. With previous knowledge from the literature, we mainly considered the kidneys, bone marrow and salivary gland toxicity as organs at risk for the potential development of side effects.

Using extrapolated organ absorbed doses, the maximum permissible activity (GBq) with [^{177}Lu]Lu-PSMA-617 to reach EBRT based organ absorbed dose limits (table 18) was calculated. This revealed varying results among patients. In patient 1 bone marrow toxicity limits were reached earlier than the kidney toxicity limits, however the whole body toxicity limit was reached at even lower activity, which might require strict

monitoring and possibly dose reduction in this patient when performing [^{177}Lu]Lu-PSMA-617 therapy. This finding is consistent with the compromised renal function and high skeletal tumor burden in this patient, which together result in a high dose to the total body.

In patient 2 bone marrow toxicity limits constrained the maximum permissible activity and the maximum number of cycles that can be administered, which is consistent with the observation already discussed in the literature that high skeletal tumor burden and can result in high bone marrow absorbed doses, which might lead to grade 1-2 hematological toxicity from [^{177}Lu]Lu-PSMA-617, especially when bone marrow function is already compromised owing to prior extensive treatment with chemotherapy/radiotherapy (Emmett et al., 2017). In the remaining three patients kidney toxicity thresholds appeared to be the dose limiting factor. The number of 6 GBq cycles keeping in view the above-mentioned dose limiting toxicities, it was found that except for patient 1, administration of up to 5 cycles of 6 GBq seems to be feasible.

Though the kidneys were an organ at risk with high organ absorbed doses, we found that in order to reach EBRT-derived dose limit of 23 Gy, a mean cumulative activity of 52 GBq can be administered. It is apparently higher than values found in literature for [^{177}Lu]Lu-PSMA-617, which were calculated to be 30 GBq by Kabasakal et al (Kabasakal et al., 2015). a difference that can be explained owing to 2D versus 3D dosimetry inherent limitations. Moreover, A. Delker et al used 3D SPECT of abdomen for dosimetric analysis of [^{177}Lu]Lu-PSMA-617 and reported a mean absorbed dose of 0.6 GY/GBq for kidneys which may allow up to 38 GBq to be administered safely (Delker et al., 2016). Use of mono-exponential non-linear least squares fit to time activity curve and a linear interpolation from time of injection in contrast to bi-exponential curve fitting and availability of dynamic data from time of injection in our current study might be the cause of this disparity between A Delker et al and our current study. Moreover, it is also believed that toxicity limit for kidneys with [^{177} Lu]Lu-PSMA-617 therapy should be increased (Emmett et al., 2017).

Considering 25 Gy as dose limit for reversible toxicity to salivary glands it was seen that even in patient 2 with highest salivary glands absorbed dose it was not a limiting factor for permissible activity calculation in that patient (Emmett et al., 2017).The

finding is supported with evidence of 4-25% occurrence of transient reversible xerostomia and dry mouth with [^{177}Lu]Lu-PSMA-617 therapy in various studies.

Our current study shows that the conversion from pre-therapeutic pharmacokinetic data obtained by [^{44}Sc]Sc-PSMA-617 PET/CT to potential normal organ absorbed doses for [^{177}Lu]Lu-PSMA-617 therapy is feasible. It might prove to be helpful in the pre-therapeutic assessment of organs at risk, which seem to be are variable among patients, and eventually aid in tailoring personalized PSMA-targeted radionuclide therapy regimens. However, further large scale studies are warranted to validate extrapolated organ doses from pre-therapeutic [^{44}Sc]Sc-PSMA-617 PET/CT with post-therapeutic [^{177}Lu]Lu-PSMA-617 dosimetry data and to correlate dosimetry results with clinical toxicity and side effects.

5 Abstract

Introduction: The availability of imaging and therapeutic radionuclides directed against same molecular targets has actualized theranostics and possibility of personalized treatment in nuclear medicine. For personalized medicine with maximum effect of therapy at target with therapeutic radionuclide, diagnostic radionuclide is required to select appropriate patient that can benefit from therapy and tailor the therapeutic doses with possible prospective dosimetric analysis for therapeutic radionuclides. Hence necessitates biodistribution and dosimetric analysis of diagnostic as well as therapeutic radionuclide. In this study, the biodistribution and dosimetric analysis of [^{68}Ga]Ga-DOTA^{ZOL} and [^{177}Lu]Lu-DOTA^{ZOL} (specific bone seeking radiopharmaceuticals) in patients with skeletal metastatic disease and [^{44}Sc]Sc-PSMA-617 (nonspecific bone seeking radiopharmaceutical) in mCRPC patients has been assessed to establish their feasible theranostic use. Further, possibility of calculation of normal organ absorbed doses for [^{177}Lu]Lu-DOTA^{ZOL} and [^{177}Lu]Lu-PSMA-617 with [^{68}Ga]Ga-DOTA^{ZOL} and [^{44}Sc]Sc-PSMA-617 respectively has been explored. **Materials and Methods:** A total of fourteen patients were enrolled for biodistribution and dosimetric analysis; five for [^{68}Ga]Ga-DOTA^{ZOL} (mean age: 72 y), four for [^{177}Lu]Lu-DOTA^{ZOL} (mean age: 69.3 y)and 05 patients for [^{44}Sc]Sc-PSMA-617 (mean age: 69 y). PET/CT scintigraphy (dynamic + static skull to mid-thigh) along with blood and urine samples for [^{68}Ga]Ga-DOTA^{ZOL} and [^{44}Sc]Sc-PSMA-617 and gamma camera planar whole body scintigraphy with blood samples collection for [^{177}Lu]Lu-DOTA^{ZOL} at multiple time points was used to determine the kinetics of respective radiopharmaceuticals. For quantitative analysis of PET/CT studies for [^{68}Ga]Ga-DOTA^{ZOL} and [^{44}Sc]Sc-PSMA-617 interview fusion software (MEDISO Medical Imaging Systems, Budapest, Hungary) was used. Percent of injected activities in source organs, blood and urine samples was used to perform kinetic analysis, residence time (MBq-h/MBq) and organ absorbed dose determination using OLINDA/EXM version 2.0 software (Hermes Medical Solutions, Stockholm, Sweden). To determine residence times and organ absorbed doses with OLINDA/EXM version 2.0 software (Hermes Medical Solutions, Stockholm, Sweden) for [^{177}Lu]Lu-DOTA^{ZOL}, percent of injected activity in source organs was determined using EANM dosimetry guidelines and methodology explained in MIRD pamphlet no 16. For prospective

dosimetric analysis the pharmacokinetic analysis of [^{68}Ga]Ga-DOTA^{ZOL} and [^{44}Sc]Sc-PSMA-617 was mathematically extrapolated for [^{177}Lu]Lu-DOTA^{ZOL} and [^{177}Lu]Lu-PSMA-617 respectively. **Results:** Biodistribution and dosimetric analysis of [^{68}Ga]Ga-DOTA^{ZOL} revealed urinary bladder as critical organ with highest absorbed dose (0.338 mSv/ MBq) and skeleton as target organ. Besides high urinary bladder and kidney absorbed doses, mean effective dose was found similar to [^{18}F]NaF. Its biodistribution was also found comparable with [^{18}F]NaF, [^{99m}Tc]Tc-MDP and [^{68}Ga]Ga-PSMA-617. Biodistribution and dosimetric analysis of [^{177}Lu]Lu-DOTA^{ZOL} showed early, high uptake in kidneys with fast clearance and gradual rise of activity in skeleton. Mean organ absorbed doses were highest in osteogenic cells (3.33 MSv/ MBq) followed by kidneys and red marrow. Maximum permissible activity was limited due to bone marrow toxicity. Prospective dosimetry with [^{68}Ga]Ga-DOTA^{ZOL} resulted in lower organ absorbed doses and lower therapeutic doses for [^{177}Lu]Lu-DOTA^{ZOL}. Biodistribution of [^{44}Sc]Sc-PSMA-617 was found similar to [^{68}Ga]Ga-PSMA but with higher organ absorbed doses and lower effective dose. Kidneys with highest radiation absorbed dose of 0.319 mSv/ MBq were the critical organs, followed by urinary bladder wall and rest of organs. Prospective dosimetric analysis of [^{177}Lu]Lu-PSMA-617 from extrapolated pharmacokinetics of [^{44}Sc]Sc-PSMA-617 revealed highest absorbed dose in the kidneys (0.44 mSv/MBq) followed by the salivary glands (0.23 mSv/MBq). The maximum permissible activity was highly variable among patients; limited by whole body absorbed dose (one patient), marrow absorbed dose (one patient) and kidney absorbed dose (three patients). **Conclusions:** [^{68}Ga]Ga-DOTA^{ZOL} and [^{177}Lu]Lu-DOTA^{ZOL} can be employed for theranostics in patients with skeletal metastatic disease. [^{68}Ga]Ga-DOTA^{ZOL} needs to be used with diuretics to reduce absorbed doses to urinary bladder and kidneys. Moreover [^{68}Ga]Ga-DOTA^{ZOL} is not appropriate for prospective dosimetric analysis of [^{177}Lu]Lu-DOTA^{ZOL}. The longer lived [^{44}Sc]Sc-PSMA-617 has been found an important theranostic radionuclide for diagnosis, follow up and probable pre-therapeutic personalized dosimetric analysis for [^{177}Lu]Lu-PSMA-617 in mCRPC patients.

6 List of illustrations

7 List of Tables

8 References

Afshar-Oromieh A, Hetzheim H, Kratochwil C, Benesova M, Eder M, Neels OC, Eisenhut M, Kubler W, Holland-Letz T, Giesel FL, Mier W, Kopka K, Haberkorn U. The Theranostic PSMA Ligand PSMA-617 in the Diagnosis of Prostate Cancer by PET/CT: Biodistribution in Humans, Radiation Dosimetry, and First Evaluation of Tumor Lesions. J. Nucl. Med 2015; 56: 1697–1705

Afshar-Oromieh A, Malcher A, Eder M, Eisenhut M, Linhart HG, Hadaschik BA, Holland-Letz T, Giesel FL, Kratochwil C, Haufe S, Haberkorn U, Zechmann CM. PET imaging with a [68Ga]gallium-labeled PSMA ligand for the diagnosis of prostate cancer: biodistribution in humans and first evaluation of tumour lesions. Eur. J. Nucl. Med. Mol. Imaging 2013; 40: 486–495

Agarwal KK, Singla S, Arora G, Bal C.177Lu-EDTMP for palliation of pain from bone metastases in patients with prostate and breast cancer: a phase II study. Eur. J. Nucl. Med. Mol. Imaging 2015; 42: 79–88

Ahmadzadehfar H. Targeted Therapy for Metastatic Prostate Cancer with Radionuclides. In: Prof. Ravinder Mohan, ed. Prostate Cancer - Leading-edge Diagnostic Procedures and Treatments. London - United Kingdom: InTech ,2016

Ahmadzadehfar H, Eppard E, Kürpig S, Fimmers R, Yordanova A, Schlenkhoff CD, Gärtner F, Rogenhofer S, Essler M. Therapeutic response and side effects of repeated radioligand therapy with 177Lu-PSMA-DKFZ-617 of castrate-resistant metastatic prostate cancer. Oncotarget 2016; 7: 12477–12488

Ahmadzadehfar H, Rahbar K, Kürpig S, Bögemann M, Claesener M, Eppard E, Gärtner F, Rogenhofer S, Schäfers M, Essler M. Early side effects and first results of radioligand therapy with 177Lu-DKFZ-617 PSMA of castrate-resistant metastatic prostate cancer: a two-centre study. EJNMMI Res 2015; 5: 114

Alavi M, Omidvari S, Mehdizadeh A, Jalilian AR, Bahrami-Samani A. Metastatic Bone Pain Palliation using 177Lu-Ethylenediaminetetramethylene Phosphonic Acid. World J Nucl Med 2015; 14: 109–115

Bal C, Arora G, Kumar P, Damle N, Das T, Chakraborty S, Banerjee S, Venkatesh M, J. Zaknun J, R.A. Pillai M. Pharmacokinetic, Dosimetry and Toxicity Study of 177 Lu-EDTMP in Patients: Phase 0/I study. Curr Radiopharm 2015; 9: 71–84

Balter H, Victoria T, Mariella T, Javier G, Rodolfo F, Andrea P, Graciela R, Juan H, Marco Eugenia D, Patricia O. 177 Lu-Labeled Agents for Neuroendocrine Tumor Therapy and Bone Pain Palliation in Uruguay. Curr Radiopharm 2015; 9: 85–93

Bander NH, Milowsky MI, Nanus DM, Kostakoglu L, Vallabhajosula S, Goldsmith SJ. Phase I trial of 177Lutetium-labeled J591, a monoclonal antibody to prostate-specific membrane antigen, in patients with androgen-independent prostate cancer. J Clin Oncol 2015; 23: 4591–4601

Baum RP, Kulkarni HR. THERANOSTICS: From Molecular Imaging Using Ga-68 Labeled Tracers and PET/CT to Personalized Radionuclide Therapy - The Bad Berka Experience. Theranostics 2012; 2: 437–447

Baum RP, Kulkarni HR, Schuchardt C, Singh A, Wirtz M, Wiessalla S, Schottelius M, Mueller D, Klette I, Wester H-J. 177Lu-Labeled Prostate-Specific Membrane Antigen Radioligand Therapy of Metastatic Castration-Resistant Prostate Cancer: Safety and Efficacy. J Nucl Med 2016; 57: 1006–1013

Benešová M, Schäfer M, Bauder-Wüst U, Afshar-Oromieh A, Kratochwil C, Mier W, Haberkorn U, Kopka K, Eder M. Preclinical Evaluation of a Tailor-Made DOTA-Conjugated PSMA Inhibitor with Optimized Linker Moiety for Imaging and Endoradiotherapy of Prostate Cancer. J Nucl Med 2015; 56: 914–920

Bentzen SM. Theragnostic imaging for radiation oncology: dose-painting by numbers. Lancet Oncol 2005; 6: 112–117

Bergmann R, Meckel M, Kubíček V, Pietzsch J, Steinbach J, Hermann P, Rösch F. 177Lu-labeled macrocyclic bisphosphonates for targeting bone metastasis in cancer treatment. EJNMMI Res 2016; 6: 5

Bolch WE, Bouchet LG, Robertson JS, Wessels BW, Siegel JA, Howell RW, Erdi AK, Aydogan B, Costes S, Watson EE, Brill AB, Charkes ND, Fisher DR, Hays MT, Thomas SR. MIRD pamphlet No. 17: the dosimetry of nonuniform activity distributions--radionuclide S values at the voxel level. J Nucl Med 1999; 40: 11S–36S

Bolch WE, Eckerman KF, Sgouros G, Thomas SR. MIRD Pamphlet No. 21: A Generalized Schema for Radiopharmaceutical Dosimetry-Standardization of Nomenclature. J Nucl Med 2009; 50: 477–484

Bozkurt MF, Özcan Z. The Evolving Role of Nuclear Medicine and Molecular Imaging: Theranostics and Personalized Therapeutic Applications. Mol Imaging Radionucl Ther 2018; 27: 1–2

Breen S, Powe J, Porter A. Dose estimation in strontium-89 radiotherapy of metastatic prostatic carcinoma. J Nucl Med 1992; 33: 1316–1324

Buscombe JR. Radionuclides in the management of thyroid cancer. Cancer Imaging 2007; 7: 202–209

Chiesa C, Sjogreen Gleisner K, Flux G, Gear J, Walrand S, Bacher K, Eberlein U, Visser EP, Chouin N, Ljungberg M, Bardiès M, Lassmann M, Strigari L, Konijnenberg MW. The conflict between treatment optimization and registration of radiopharmaceuticals with fixed activity posology in oncological nuclear medicine therapy. Eur J Nucl Med Mol Imaging 2017; 44: 1783–1786

Cuccurullo V, Cascini GL, Tamburrini O, Rotondo A, Mansi L. Bone metastases radiopharmaceuticals: an overview. Curr Radiopharm 2013; 6: 41–47

Dash A, Knapp FF, Pillai M. Targeted Radionuclide Therapy - An Overview. Curr Radiopharm 2013; 6: 152–180

Dash A, Pillai MRA, Knapp FF. Production of 177Lu for Targeted Radionuclide Therapy: Available Options. Nucl Med Mol Imaging 2015; 49: 85–107

Delker A, Fendler WP, Kratochwil C, Brunegraf A, Gosewisch A, Gildehaus FJ, Tritschler S, Stief CG, Kopka K, Haberkorn U, Bartenstein P, Böning G. Dosimetry for 177Lu-DKFZ-PSMA-617: a new radiopharmaceutical for the treatment of metastatic prostate cancer. Eur J Nucl Med Mol Imaging 2016; 43: 42–51

Eberlein U, Cremonesi M, Lassmann M. Individualized Dosimetry for Theranostics: Necessary, Nice to Have, or Counterproductive?. J Nucl Med 2017; 58: 97S–103S

Ebetino FH, Hogan AML, Sun S, Tsoumpra MK, Duan X, Triffitt JT, Kwaasi AA, Dunford JE, Barnett BL, Oppermann U, Lundy MW, Boyde A, Kashemirov BA, McKenna CE, Russell RGG. The relationship between the chemistry and biological activity of the bisphosphonates. Bone 2011; 49: 20–33

Emmett L, Willowson K, Violet J, Shin J, Blanksby A, Lee J.Lutetium 177 PSMA radionuclide therapy for men with prostate cancer: a review of the current literature and discussion of practical aspects of therapy. J Med Radiat. Sci 2017; 64: 52–60

Eppard E, de la Fuente2 A, Benešová M, Khawar A, Bundschuh RA, Gärtner FC, Kreppel B, Kopka K, Essler M, Rösch F. Clinical translation and first in-human use of [44Sc]Sc-PSMA-617 for pet imaging of metastasized castrate-resistant prostate cancer. Theranostics 2017; 7: 4359–4369

Erdi YE, Macapinlac H, Larson SM, Erdi AK, Yeung H, Furhang EE, Humm JL. Radiation Dose Assessment for I-131 Therapy of Thyroid Cancer Using I-124 PET Imaging. Clin Positron Imaging 1999; 2: 41–46

Fellner M, Baum RP, Kubíček V, Hermann P, Lukeš I, Prasad V, Rösch F. PET/CT imaging of osteoblastic bone metastases with 68Ga- bisphosphonates: First human study. Eur J Nucl Med Mol Imaging 2010; 37: 834

Fellner M, Biesalski B, Bausbacher N, Kubícek V, Hermann P, Rösch F, Thews O. (2012) 68Ga-BPAMD: PET-imaging of bone metastases with a generator based positron emitter. Nucl Med Biol 2012. 39: 993–999

Fellner M, Riss P, Loktionova NS, Zhernosekov KP, Thews O, Geraldes CFGC, Kovacs Z, Lukes, Rösch F. Comparison of different phosphorus-containing ligands complexing 68Ga for PET-imaging of bone metabolism. Radiochim Acta 2011; 99: 43–51

Fendler WP, Reinhardt S, Ilhan H, Delker A, Böning G, Gildehaus FJ, Stief C, Bartenstein P, Gratzke C, Lehner S, Rominger A. Preliminary experience with dosimetry, response and patient reported outcome after 177Lu-PSMA-617 therapy for metastatic castration-resistant prostate cancer. Oncotarget 2017; 8: 3581–3590

Fischer M, Kampen WU. Radionuclide Therapy of Bone Metastases. Breast Care (Basel) 2012; 7: 100–107

Flux GD, Sjogreen Gleisner K, Chiesa C, Lassmann M, Chouin N, Gear J, Bardiès M, Walrand S, Bacher K, Eberlein U, Ljungberg M, Strigari L, Visser E, Konijnenberg MW. From fixed activities to personalized treatments in radionuclide therapy: lost in translation?. Eur J Nucl Med Mol Imaging 2018; 45: 152–154

Gaertner FC, Halabi K, Ahmadzadehfar H, Kürpig S, Eppard E, Kotsikopoulos C, Liakos N, Bundschuh RA, Strunk H, Essler M. Uptake of PSMA-ligands in normal tissues is dependent on tumor load in patients with prostate cancer. Oncotarget 2017; 8: 55094-55103

Herrmann K, Bluemel C, Weineisen M, Schottelius M, Wester H-JH-J, Czernin J, Eberlein U, Beykan S, Lapa C, Riedmiller H, Krebs M, Kropf S, Schirbel A, Buck AK, Lassmann M. Biodistribution and Radiation Dosimetry for a Probe Targeting Prostate-Specific Membrane Antigen for Imaging and Therapy. J Nucl Med 2015. 56: 855–861

Hindorf C, Lindén O, Tennvall J, Wingårdh K, Strand SE. Evaluation of methods for red marrow dosimetry based on patients undergoing radioimmunotherapy. Acta Oncol. (Madr) 2005; 44: 579–588

Holub J, Meckel M, Kubíček V, Rösch F, Hermann P. Gallium(III) complexes of NOTA-bis (phosphonate) conjugates as PET radiotracers for bone imaging. Contrast Media Mol. Imaging 2015; 10: 122–134

ICRP. Basic anatomical and physiological data for use in radiological protection - the skeleton. ICRP Publication 70. Ann. ICRP 1995; 25(2)

ICRP. Radiation Dose to Patients from Pharmaceuticals - Addendum 3 to ICRP Publication 53. ICRP publication 106. Ann. ICRP 2008 ;38:1–197

Intenzo CM, Jabbour S, Lin HC, Miller JL, Kim SM, Capuzzi DM, Mitchell EP. Scintigraphic Imaging of Body Neuroendocrine Tumors. Radio Graphics 2007; 27: 1355–1369

Kabasakal L, Abuqbeitah M, Aygün A, Yeyin N, Ocak M, Demirci E, Toklu T, Aygün A, Yeyin N, Ocak M, Demirci E, Toklu T. Pre-therapeutic dosimetry of normal organs and tissues of 177Lu-PSMA-617 prostate-specific membrane antigen (PSMA) inhibitor in patients with castration-resistant prostate cancer. Eur J Nucl Med Mol Imaging 2015; 42: 1976–1983

Kesavan M, Turner JH, Meyrick D, Yeo S, Cardaci G, Lenzo NP. Salvage Radiopeptide Therapy of Advanced Castrate-Resistant Prostate Cancer with Lutetium-177-Labeled Prostate-Specific Membrane Antigen: Efficacy and Safety in Routine Practice. Cancer Biother Radiopharm 2018; 33: 274–281

Kratochwil C, Giesel FL, Stefanova M, Bene ova M, Bronzel M, Afshar-Oromieh A, Mier W, Eder M, Kopka K, Haberkorn U. PSMA-Targeted Radionuclide Therapy of Metastatic Castration-Resistant Prostate Cancer with 177Lu-Labeled PSMA-617. J Nucl Med 2016. 57: 1170–1176

Kulkarni HR, Singh A, Schuchardt C, Niepsch K, Sayeg M, Leshch Y, Wester H-J, Baum RP. PSMA-Based Radioligand Therapy for Metastatic Castration-Resistant Prostate Cancer: The Bad Berka Experience Since 2013. J Nucl Med 2016; 57: 97S–104S

Kurdziel KA, Shih JH, Apolo AB, Lindenberg L, Mena E, McKinney YY, Adler SS, Turkbey B, Dahut W, Gulley JL, Madan RA, Landgren O, Choyke PL. The kinetics and reproducibility of 18F-sodium fluoride for oncology using current PET camera technology. J Nucl Med 2012; 53: 1175–1184

Lassmann M, Eberlein U. The relevance of dosimetry in precision medicine. J. Nucl. Med 2018;59: 1494–1499

Ljungberg M, Sjögreen Gleisner K. Personalized Dosimetry for Radionuclide Therapy Using Molecular Imaging Tools. Biomedicines 2016; 4: 25

Luckman SP, Hughes DE, Coxon FP, Russell RGG, Rogers MJ. Nitrogen-Containing Bisphosphonates Inhibit the Mevalonate Pathway and Prevent Post-Translational Prenylation of GTP-Binding Proteins, Including Ras. J Bone Miner Res 1998; 13: 581–589

Lütje S, Heskamp S, Cornelissen AS, Poeppel TD, van den Broek SAMW, Rosenbaum-Krumme S, Bockisch A, Gotthardt M, Rijpkema M, Boerman OC. PSMA ligands for radionuclide imaging and therapy of prostate cancer: Clinical status. Theranostics 2015; 5: 1388–1401

Macedo F, Ladeira K, Pinho F, Saraiva N, Bonito N, Pinto L, Goncalves F. Bone Metastases: An Overview. Oncol Rev 2017; 11: 321

Mazzarri S, Guidoccio F, Mariani G. The emerging potential of 177Lu-EDTMP: an attractive novel option for radiometabolic therapy of skeletal metastases. Clin Transl Imaging 2015; 3: 167–168

Meckel M, Bergmann R, Miederer M, Roesch F. Bone targeting compounds for radiotherapy and imaging: *Me(III)-DOTA conjugates of bisphosphonic acid, pamidronic acid and zoledronic acid. EJNMMI Radiopharm Chem 2017; 1: 14

Montalvetti A, Bailey BN, Martin MB, Severin GW, Oldfield E, Docampo R. Bisphosphonates Are Potent Inhibitors of Trypanosoma cruzi Farnesyl Pyrophosphate Synthase. J Biol Chem 2001; 276: 33930–33937

Nagarajah J, Janssen M, Hetkamp P, Jentzen W. Iodine Symporter Targeting with 124I/131I Theranostics. J Nucl Med 2017; 58: 34S–38S

Nikzad M, Jalilian AR, Shirvani-Arani S, Bahrami-Samani A, Golchoubian H. Production, quality control and pharmacokinetic studies of 177Lu-zoledronate for bone pain palliation therapy. J Radioanal Nucl Chem 2013; 298: 1273–1281

O'Sullivan GJ, Carty FL, Cronin CG. Imaging of bone metastasis: An update. World J Radiol 2015; 7: 202–211

Okamoto S, Thieme A, Allmann J, D'Alessandria C, Maurer T, Retz M, Tauber R, Heck MM, Wester H-J, Tamaki N, Fendler WP, Herrmann K, Pfob CH, Scheidhauer K, Schwaiger M, Ziegler S, Eiber M. Radiation Dosimetry for 177Lu-PSMA I &T in Metastatic Castration-Resistant Prostate Cancer: Absorbed Dose in Normal Organs and Tumor Lesions. J Nucl Med 2017; 58: 445–450

Pandit-Taskar N, Batraki M, Divgi CR. Radiopharmaceutical therapy for palliation of bone pain from osseous metastases. J Nucl Med 2004; 45: 1358–1365

Passah A, Tripathi M, Ballal S, Yadav MP, Kumar R, Roesch F, Meckel M, Chakraborty PS, Bal C, Sarathi Chakraborty P, Bal C. Evaluation of bone-seeking novel radiotracer 68Ga-NO2AP-Bisphosphonate for the detection of skeletal metastases in carcinoma breast. Eur J Nucl Med Mol Imaging 2017; 44: 41– 49

Pfannkuchen N, Bausbacher N, Pektor S, Miederer M, Rosch F. In vivo Evaluation of [225 Ac]Ac-DOTA ZOL for α-Therapy of Bone Metastases. Curr Radiopharm 2018; 11: 223–230

Pfannkuchen N, Meckel M, Bergmann R, Bachmann M, Bal C, Sathekge M, Mohnike W,

Baum RP, Rösch F. Novel radiolabeled bisphosphonates for PET diagnosis and endoradiotherapy of bone metastases. Pharmaceuticals (Basel) 2017; 10

Pfestroff A, Luster M, Jilg CA, Olbert PJ, Ohlmann CH, Lassmann M, Maecke HR, Ezziddin S, Bodei L. Current status and future perspectives of PSMA-targeted therapy in Europe: opportunity knocks. Eur J Nucl Med Mol Imaging 2015; 42: 1971–1975

Pfob CH, Ziegler S, Graner FP, Köhner M, Schachoff S, Blechert B, Wester HJ, Scheidhauer K, Schwaiger M, Maurer T, Eiber M. Biodistribution and radiation dosimetry of 68Ga-PSMA HBED CC???a PSMA specific probe for PET imaging of prostate cancer. Eur J Nucl Med Mol Imaging 2016; 43: 1962–1970

Pruszyński M, Majkowska-Pilip A, Loktionova NS, Eppard E, Roesch F. Radiolabeling of DOTATOC with the long-lived positron emitter 44Sc. Appl Radiat Isot 2012; 70: 974–979

Qu X, Huang X, Yan W, Wu L, Dai K. A meta-analysis of 18FDG-PET-CT, 18FDG-PET, MRI and bone scintigraphy for diagnosis of bone metastases in patients with lung cancer. Eur J Radiol 2012; 81: 1007–1015

Rahbar K, Ahmadzadehfar H, Kratochwil C, Haberkorn U, Schäfers M, Essler M, Baum RP, Kulkarani HR, Schmidt M, Bartenstein P, Pfestroff A, Lützen U, Marx M, Prasad V, Brenner W, Heinzel A, Ruf J, Meyer PT, Heuschkel M, Eveslage M, Bögemann M, Fendler WP, Krause BJ. German multicenter study investigating 177Lu-PSMA-617 radioligand therapy in advanced prostate cancer patients. J Nucl Med 2016a; 58: 85–91

Rahbar K, Schmidt M, Heinzel A, Eppard E, Bode A, Yordanova A, Claesener M & Ahmadzadehfar H. Response and tolerability of a single dose of 177Lu-PSMA-617 in patients with metastatic castration-resistant prostate cancer: a multicenter retrospective analysis. J Nucl Med 2016b; 57: 1334–1339

Rösch F, Baum RP. Generator-based PET radiopharmaceuticals for molecular imaging of tumours: on the way to THERANOSTICS. Dalton Trans 2011; 40: 6104–11

Rösch F, Herzog H, Qaim SM. The beginning and development of the theranostic approach in nuclear medicine, as exemplified by the radionuclide pair 86Y and 90Y. Pharmaceuticals 2017; 10: 1–28

Russell RGG. Bisphosphonates: Mode of Action and Pharmacology. Pediatrics 2007; 119: S150–S162

Scarpa L, Buxbaum S, Kendler D, Fink K, Bektic J, Gruber L, Decristoforo C, Uprimny C, Lukas P, Horninger W, Virgolini I. The 68Ga/177Lu theragnostic concept in PSMA targeting of castration-resistant prostate cancer: correlation of SUVmax values and absorbed dose estimates. Eur J Nucl Med Mol Imaging 2017; 44: 788–800

Serafini AN. Therapy of metastatic bone pain. J Nucl Med 2001; 42: 895–906

Sgouros G, Stabin M, Erdi Y, Akabani G, Kwok C, Brill AB, Wessels B. Red marrow dosimetry for radiolabeled antibodies that bind to marrow, bone, or blood components. Med. Phys 2000; 27: 2150–2164

Sharma S, Singh B, Koul A, Mittal BR. Comparative Therapeutic Efficacy of 153Sm-EDTMP and 177Lu-EDTMP for Bone Pain Palliation in Patients with Skeletal Metastases: Patients' Pain Score Analysis and Personalized Dosimetry. Front. Med 2017; 4: 46

Shen S, DeNardo GL, Sgouros G, O'Donnell RT, DeNardo. SJ. Practical determination of patient-specific marrow dose using radioactivity concentration in blood and body. J Nucl Med 1999; 40: 2102–2106

Shinto AS, Shibu D, Kamaleshwaran KK, Das T, Chakraborty S, Banerjee S, Thirumalaisamy P, Das P, Veersekar G. 177Lu-EDTMP for treatment of bone pain in patients with disseminated skeletal metastases. J Nucl Med Technol 2014; 42: 55–61

Siegel J. Establishing a clinically meaningful predictive model of hematologic toxicity in nonmyeloablative targeted radiotherapy: practical aspects and limitations of red marrow dosimetry. Cancer Biother Radiopharm 2005; 20: 126–140

Siegel J, Thomas SR, Stubbs JB, Stabin MG, Hays MT, Koral KF, Robertson JS, Howell RW, Wessels BW, Fisher DR, Weber DA, Brill AB. MIRD pamphlet no. 16: techniques for quantitative radio pharmaceutical biodistribution data acquisition and analysis for use in human radiation dose estimates. J Nucl Med 1999; 40: 37S–61S

Singh A, van der Meulen NP, Müller C, Klette I, Kulkarni HR, Türler A, Schibli R, Baum RP. First-in-Human PET/CT Imaging of Metastatic Neuroendocrine Neoplasms with Cyclotron-Produced 44 Sc-DOTATOC: A Proof-of-Concept Study. Cancer Biother Radiopharm 2017; 32: 124–132

Stabin MG. Fundamentals of nuclear medicine dosimetry. NewYork: Springer, 2008

Strigari L, Konijnenberg M, Chiesa C, Bardies M, Du Y, Gleisner KS, Lassmann M, Flux G. The evidence base for the use of internal dosimetry in the clinical practice of molecular radiotherapy. Eur J Nucl Med Mol Imaging 2014; 41: 1976–1988

Taïeb D, Hicks RJ, Pacak K. Nuclear Medicine in Cancer Theranostics: Beyond the Target. J Nucl Med 2016; 57: 1659–1660

Thapa P, Nikam D, Das T, Sonawane G, Agarwal JP, Basu S. Clinical Efficacy and Safety Comparison of 177Lu-EDTMP with 153Sm-EDTMP on an Equidose Basis in

Patients with Painful Skeletal Metastases. J Nucl Med 2015; 56: 1513–1519

Umbricht CA, Benešová M, Schmid RM, Türler A, Schibli R, van der Meulen NP, Müller C. 44Sc-PSMA-617 for radiotheragnostics in tandem with 177Lu-PSMA-617—preclinical investigations in comparison with 68Ga-PSMA-11 and 68Ga-PSMA-617. EJNMMI Res 2017; 7: 9

Urhan M, Dadparvar S, Mavi A, Houseni M, Chamroonrat W, Alavi A, Mandel SJ. Iodine-123 as a diagnostic imaging agent in differentiated thyroid carcinoma: a comparison with iodine-131 post-treatment scanning and serum thyroglobulin measurement. Eur J Nucl Med Mol Imaging 2007; 34: 1012–1017

Verburg FA, Heinzel A, Hänscheid H, Mottaghy FM, Luster M, Giovanella L. Nothing new under the nuclear sun: Towards 80 years of theranostics in nuclear medicine. Eur J Nucl Med Mol Imaging 2014; 41: 199–201

Hernandez RK, Adhia A, Wade SW, O'Connor E, Arellano J, Francis K, Alvrtsyan H, Million R, Liede A. Prevalence of bone metastases and bone-targeting agent use among solid tumor patients in the United States. Clin Epidemiol 2015; 7: 335–345

Walker RC, Smith GT, Liu E, Moore B, Clanton J, Stabin M. Measured Human Dosimetry of 68Ga-DOTATATE. J Nucl Med 2013; 54: 855–860

Wright CL, Zhang J, Tweedle MF, Knopp M V, Hall NC. Theranostic Imaging of Yttrium-90. Biomed Res Int 2015; 2015: 481279

Yang H-L, Liu T, Wang X-M, Xu Y, Deng S-M. Diagnosis of bone metastases: a meta-analysis comparing 18FDG PET, CT, MRI and bone scintigraphy. Eur Radiol 2011; 21: 2604–2617

Yordanova A, Becker A, Eppard E, Kürpig S, Fisang C, Feldmann G, Essler M. Ahmadzadehfar H. The impact of repeated cycles of radioligand therapy using [177Lu]Lu-PSMA-617 on renal function in patients with hormone refractory metastatic prostate cancer. Eur. J. Nucl. Med. Mol. Imaging 2017a; 44: 1473–1479

Yordanova A, Eppard E, Kürpig S, Bundschuh RA, Schönberger S, Gonzalez-Carmona M, Feldmann G, Ahmadzadehfar H, Essler M. Theranostics in nuclear medicine practice. Onco. Targets. Ther 2017b; 10: 4821–4828

Yousefnia H, Zolghadri S, Jalilian AR. Absorbed dose assessment of (177)Lu-zoledronate and 177Lu-EDTMP for human based on biodistribution data in rats. J Med Phys 2015; 40: 102–108

Yuan J, Liu C, Liu X, Wang Y, Kuai D, Zhang G, Zaknun JJ. Efficacy and Safety of

177Lu-EDTMP in Bone Metastatic Pain Palliation in Breast Cancer and Hormone Refractory Prostate Cancer. Clin Nucl Med 2013; 38: 88–92

Zechmann CM, Afshar-Oromieh A, Armor T, Stubbs JB, Mier W, Hadaschik B, Joyal J, Kopka K, Debus J, Babich JW, Haberkorn U. Radiation dosimetry and first therapy results with a 124I/ 131I-labeled small molecule (MIP-1095) targeting PSMA for prostate cancer therapy. Eur J Nucl Med Mol Imaging 2014; 41: 1280–1292